

1 **Title:** Differential encoding of mammalian proprioception by voltage-gated sodium channels

2 **Short Title:** Encoding of proprioception by sodium channels

3  
4 **Authors**

5 Cyrrus M. Espino<sup>1</sup>, Chetan Nagaraja<sup>1</sup>, Serena Ortiz<sup>2</sup>, Jacquelyn R. Dayton<sup>1</sup>, Akash R. Murali<sup>1,4</sup>,  
6 Yanki Ma<sup>1,4</sup>, Emari L. Mann<sup>1,5</sup>, Snigdha Garlapalli<sup>1,6</sup>, Ross P. Wohlgemuth<sup>3</sup>, Sarah E. Brashear<sup>3</sup>,  
7 Lucas R. Smith<sup>3</sup>, Katherine A. Wilkinson<sup>2</sup>, Theanne N. Griffith<sup>1\*</sup>

8  
9 **Affiliations**

10 <sup>1</sup>Department of Physiology and Membrane Biology, University of California, Davis, Davis, CA,  
11 USA

12 <sup>2</sup>Department of Biological Sciences, San José State University, San Jose, CA, USA

13 <sup>3</sup>Department of Physiology, Neurobiology, and Behavior, University of California, Davis, Davis,  
14 CA, USA

15 <sup>4</sup>Undergraduate Program in Neurobiology, Physiology and Behavior, University of California,  
16 Davis, Davis, CA, USA

17 <sup>5</sup>Postbaccalaureate Research Education Program at UC Davis, University of California, Davis,  
18 Davis, CA, USA

19 <sup>6</sup>Undergraduate Program in Psychology, University of California, Davis, Davis, CA, USA

20  
21 \*Corresponding Author: Theanne N. Griffith

22 1275 Med Science Drive

23 Tupper Hall 4135

24 Davis, CA 95616

25 530.754.2780

26 tgriffith@ucdavis.edu

28 **Abstract**

29 Animals that require purposeful movement for survival are endowed with mechanosensory neurons  
30 called proprioceptors that provide essential sensory feedback from muscles and joints to spinal cord  
31 circuits, which modulates motor output. Despite the essential nature of proprioceptive signaling in  
32 daily life, the mechanisms governing proprioceptor activity are poorly understood. Here, we have  
33 identified distinct and nonredundant roles for two voltage-gated sodium channels (Navs), Nav1.1  
34 and Nav1.6, in mammalian proprioception. Deletion of Nav1.6 in somatosensory neurons  
35 (Nav1.6<sup>ckO</sup> mice) causes severe motor deficits accompanied by complete loss of proprioceptive  
36 transmission, which contrasts with our previous findings using similar mouse models to target  
37 Nav1.1 (Nav1.1<sup>ckO</sup>). In Nav1.6<sup>ckO</sup> animals, loss of proprioceptive feedback caused non-cell-  
38 autonomous impairments in proprioceptor end-organs and skeletal muscle that were absent in  
39 Nav1.1<sup>ckO</sup> mice. We attribute the differential contribution of Nav1.1 and Nav1.6 in proprioceptor  
40 function to distinct cellular localization patterns. Collectively, these data provide the first evidence  
41 that Nav subtypes uniquely shape neurotransmission within a somatosensory modality.

42 **Teaser**

43 Voltage gated sodium channels differentially encode mammalian proprioception via distinct  
44 cellular localization patterns.

45

## 46 **Introduction**

47 Proprioception, often referred to as our “sixth sense”, is a largely unconscious sensation that allows  
48 for the detection of one’s own body position and movement in space (1, 2). Proprioceptive signaling  
49 is initiated by a subclass of peripheral mechanosensory neurons, called proprioceptors, whose cell  
50 bodies reside in the dorsal root ganglia (DRG) or mesencephalic trigeminal nucleus (1, 3, 4). The  
51 peripheral axons of proprioceptors innervate skeletal muscle and form mechanosensitive end  
52 organs, referred to as muscle spindles and Golgi tendon organs, which are activated by changes in  
53 muscle length or force, respectively (1). In proprioceptors, the mechanosensitive ion channel Piezo2  
54 transduces changes in muscle movement into electrical signals that give rise to sustained trains of  
55 action potentials, which are subsequently transmitted to spinal cord circuits (4, 5). Indeed, patients  
56 harboring Piezo2 loss-of-function mutations have impaired proprioception in the absence of visual  
57 input (6). Recently, we determined that the voltage-gated sodium channel (Nav), Nav1.1, is also  
58 essential for mammalian proprioception, and plays a specific role in maintaining proprioceptor  
59 firing during sustained muscle stretch (7). Furthermore, we determined Nav1.1 to be  
60 haploinsufficient for proprioceptor function and motor behaviors, which is consistent with the  
61 clinical manifestations associated with the thousands of human disease-causing mutations  
62 associated with its gene, *Scn1a*. Surprisingly, Nav1.1 was not required for muscle proprioceptor  
63 responses to dynamic muscle movement or vibration. This raises the question as to whether Navs  
64 play distinct roles in encoding proprioceptive signals.

65

66 In addition to Nav1.1, proprioceptors also express Nav1.6 and Nav1.7 (7). Nav1.7 is most notable  
67 for its role in pain signaling, whereby gain- or loss-of-function mutations in *Scn9a*, the gene  
68 encoding Nav1.7, cause congenital hypersensitivity or insensitivity to pain, respectively (8, 9) .  
69 Mice and humans lacking Nav1.7, however, do not have reported motor deficits, indicating a  
70 limited role for this channel in proprioception at the behavioral level (9, 10). Conversely, the gene

71 encoding Nav1.6, *Scn8a*, is linked to various pathophysiological conditions associated with motor  
72 impairments, such as developmental epileptic encephalopathy and ataxia (11). Furthermore, global  
73 inactivation of *Scn8a* in mice leads to hind limb paralysis and death by postnatal day (P) 21 (12).  
74 In cerebellar Purkinje neurons, loss of Nav1.6 significantly reduces spontaneous activity and leads  
75 to impairments in motor coordination (13). While these data highlight critical roles for Nav1.6 in  
76 brain-mediated motor control, Nav1.6 function remains understudied in the peripheral nervous  
77 system, and how this channel contributes to proprioception is unknown. Importantly, understanding  
78 the unique contributions of Navs to peripheral proprioception will enhance our mechanistic  
79 understanding of the sensorimotor phenotypes associated with various Nav channelopathies.

80  
81 In the present study, we set out to determine whether Navs plays distinct or redundant roles in  
82 proprioceptive signaling, focusing on the contributions of Nav1.1 and Nav1.6. The use of a *Pvalb*-  
83 *Cre* mouse line to drive Nav deletion in proprioceptors is not feasible due to parvalbumin expression  
84 in the brain and spinal cord (7, 14, 15). Thus, we used a somatosensory-neuron wide genetic  
85 targeting strategy to conditionally deleted Nav1.6 (*Pirt<sup>Cre/+</sup>;Scn8a<sup>fl/fl</sup>*, Nav1.6<sup>cKO</sup>) and found this  
86 resulted in severe impairments in motor coordination that were phenotypically distinct from those  
87 we previously observed in mice lacking Nav1.1 in somatosensory neurons (*Pirt<sup>Cre/+</sup>;Scn1a<sup>fl/fl</sup>*,  
88 Nav1.1<sup>cKO</sup>, 7). In line with behavioral observations, *ex vivo* proprioceptor muscle-nerve recordings  
89 showed neurotransmission in response to both dynamic and static muscle movement was abolished  
90 in the absence of Nav1.6, which contrasts with our prior finding of a selective role for Nav1.1 in  
91 proprioceptor encoding of static muscle stretch. Electrophysiological recordings of the  
92 proprioceptor-mediated monosynaptic reflex in the spinal cord further confirmed an essential, albeit  
93 developmentally dependent, role for Nav1.6 in proprioceptor synaptic function, whereas Nav1.1  
94 was found to be dispensable. Nav1.6<sup>cKO</sup> mice also exhibited abnormal muscle spindle end organ  
95 structure, which was not observed in Nav1.1<sup>cKO</sup> mice, suggesting severely but not moderately

96 impaired proprioceptive signaling interferes with proprioceptor end organ development.  
97 Surprisingly, we also observed non-cell-autonomous deficits in skeletal muscle development in  
98 Nav1.6<sup>cKO</sup> mice, but not Nav1.1<sup>cKO</sup> mice, that are suggestive of blocked hypertrophy during  
99 development. Finally, cellular localization experiments found Nav1.1 and Nav1.6 occupy discrete  
100 excitable domains in proprioceptor muscle spindles, which we predict underlies their unique roles  
101 in electrical transmission.

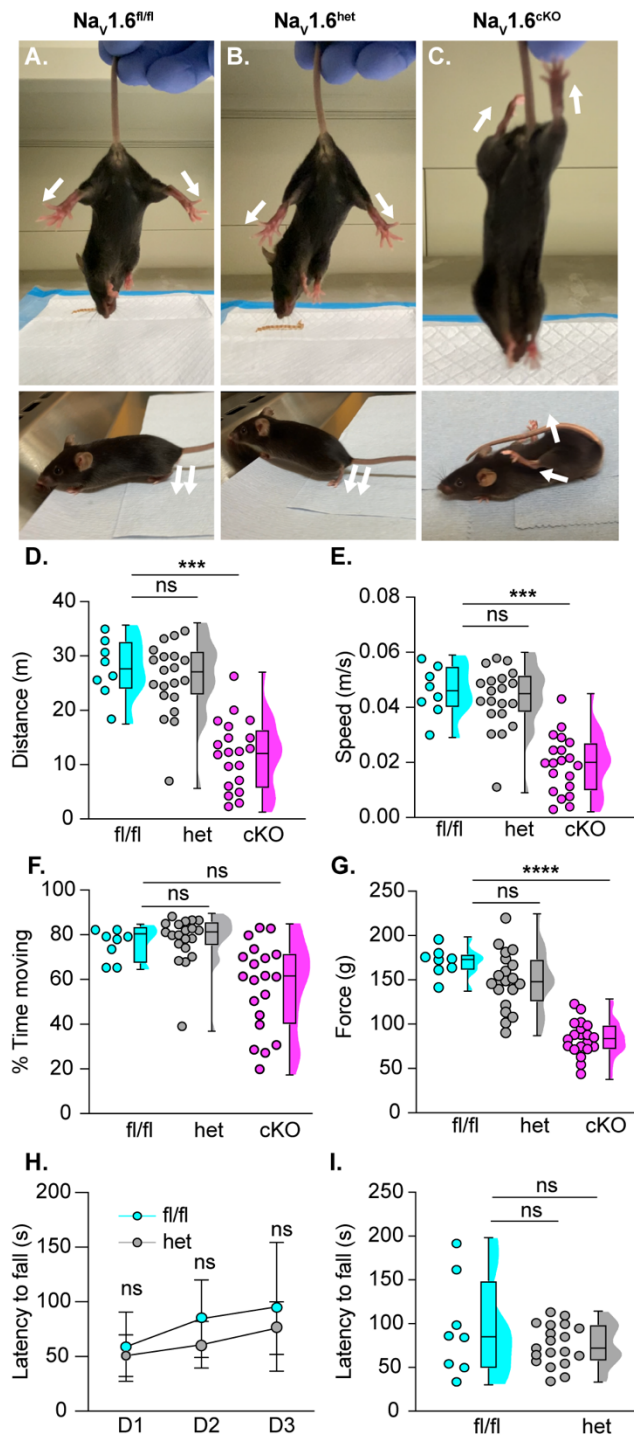
102

103 Collectively, our findings reveal that Nav1.1 and Nav1.6 are both essential to proprioceptive  
104 signaling but have independent and non-redundant functions. The differential contribution of  
105 Nav1.1 and Nav1.6 to the activity of individual somatosensory neuron subtypes has not been  
106 investigated, and we hypothesize our findings are broadly applicable to other somatosensory  
107 neurons that rely on these channels for neuronal signaling.

108

109 **Results**

110



111 **Fig. 1. Nav1.6 is required for somatosensory neuron-driven motor behaviors and function.**  
 112 Representative images showing limb position of adult  $Na_v1.6^{fl/fl}$  (A),  $Na_v1.6^{het}$  (B), and  $Na_v1.6^{cKO}$   
 113 (C) mice suspended from the tail (above) and on flat surface (below). White arrows indicate the  
 114 direction of hind limbs. Quantification of distance traveled (D,  $Na_v1.6^{het}$   $p > 0.999$ ,  $Na_v1.6^{cKO}$   $p =$   
 115  $0.0003$ , compared to  $Na_v1.6^{fl/fl}$ ), average speed (E,  $Na_v1.6^{het}$   $p > 0.999$ ,  $Na_v1.6^{cKO}$   $p = 0.0003$ ),  
 116 and the percent of time spent moving (F,  $Na_v1.6^{het}$   $p > 0.999$ ,  $Na_v1.6^{cKO}$   $p = 0.05$ , compared to  
 117  $Na_v1.6^{fl/fl}$ ) for  $Na_v1.6^{fl/fl}$  (cyan),  $Na_v1.6^{het}$  (grey), and  $Na_v1.6^{cKO}$  (magenta) mice as measured in  
 118 the open field assay for a 10-minute testing period. (G) Average grip force in grams measured

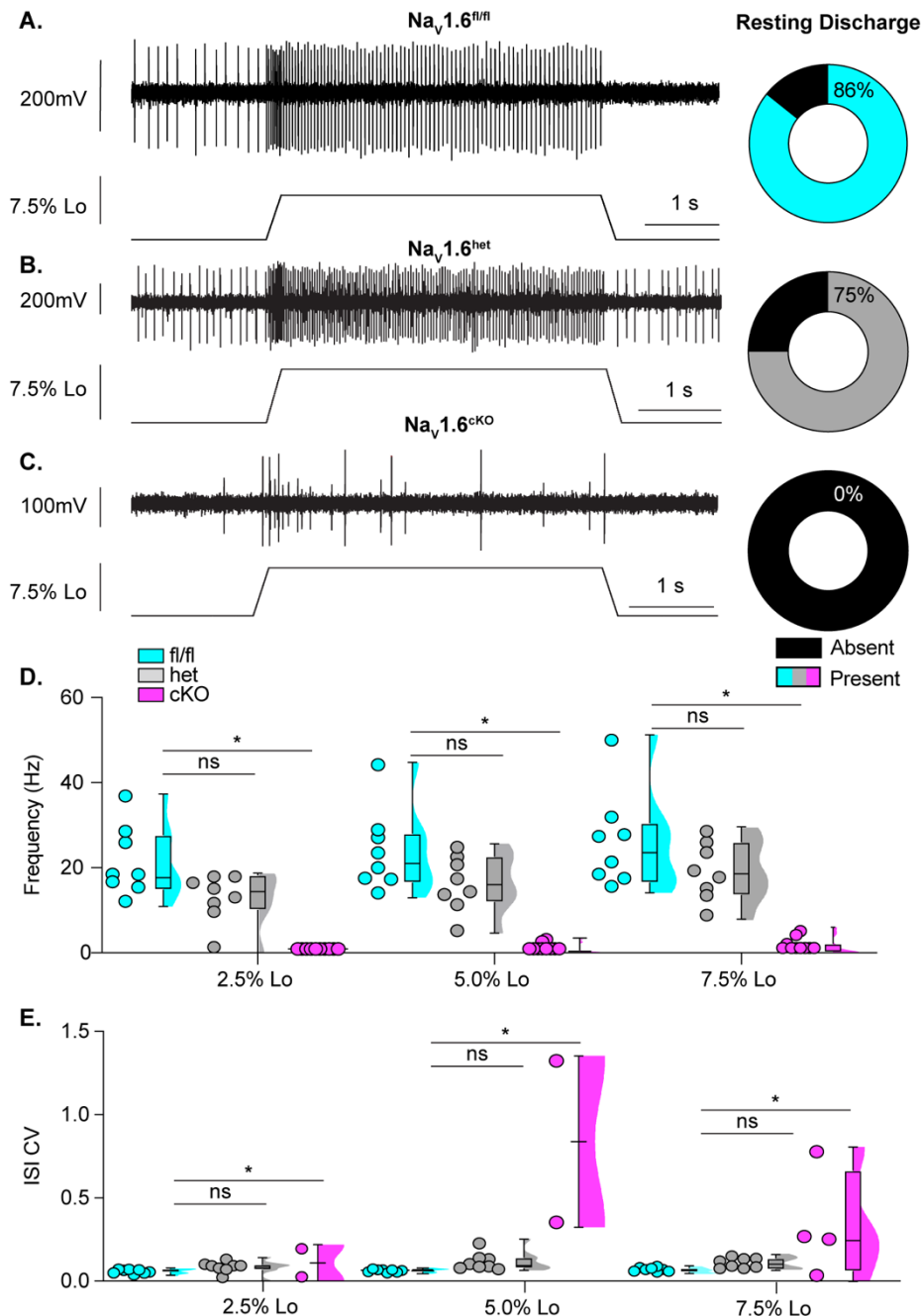
119 across 6 consecutive trials; Nav1.6<sup>het</sup>  $p = 0.4947$ , Nav1.6<sup>cKO</sup>  $p < 0.0001$ , compared to Nav1.6<sup>fl/fl</sup>.  
120 **(H)** Average latency to fall from the rotarod across three consecutive training days. No statistically  
121 significant genotype-dependent difference was observed ( $p = 0.1342$ ). **(I)** Average latency to fall  
122 on third day of testing (Nav1.6<sup>het</sup>  $p = 0.3943$ , compared to Nav1.6<sup>fl/fl</sup>). Each dot represents one  
123 animal, except in **(H)** where each dot represents the mean across animals. Box and whisker plots  
124 represent maximum, minimum, median, upper and lower quartiles of data sets. A Kruskal-Wallis  
125 test with Dunn's multiple comparisons **(D to G)**, a Two-way ANOVA with Sidak's multiple  
126 comparisons **(H)**, and a Welch's T-test **(I)** were used to determine statistical significance. Nav1.6<sup>fl/fl</sup>  
127  $N = 8$ , Nav1.6<sup>het</sup>  $N=20$ , Nav1.6<sup>cKO</sup>  $N=20$ .

## 128 **Genetic ablation of Nav1.6 in sensory neurons leads to profound motor coordination deficits.**

130 To examine the *in vivo* role of Nav1.6 in sensory-driven motor behaviors, we generated a mouse  
131 line in which Nav1.6 is deleted in all peripheral sensory neurons: *Pirt*<sup>Cre/+</sup>*Scn8a*<sup>fl/fl</sup> (hereafter  
132 referred to as Nav1.6<sup>cKO</sup>), an approach we previously used to investigate Nav1.1 function in  
133 proprioception (7). While not selective to proprioceptors, this approach avoids significant off-target  
134 effects on the central nervous system, which include premature death and seizures (14). Nav1.6<sup>cKO</sup>  
135 mice displayed extreme motor deficits that were absent in mice retaining a single copy (Nav1.6<sup>het</sup>)  
136 or both copies (Nav1.6<sup>fl/fl</sup>) of *Scn8a* (Fig. 1). Motor deficits included abnormal hind limb position  
137 when suspended by the tail (Fig. 1 A to C, top; movie S1) or when placed on a flat surface (Fig. 1  
138 A to C, bottom; movie S2) and an inability to use the tail to guide movements. The motor phenotype  
139 produced by Nav1.6 deletion was more severe than the phenotype we observed following deletion  
140 of Nav1.1 in sensory neurons (*Pirt*<sup>Cre/+</sup>;*Scn1a*<sup>fl/fl</sup>, Nav1.1<sup>cKO</sup>, 7). Interestingly, however, Nav1.6<sup>cKO</sup>  
141 mice did not display the tremor-like movements we previously observed in Nav1.1<sup>cKO</sup> animals,  
142 highlighting a behaviorally distinct phenotype between the two models. We quantified spontaneous  
143 locomotion in the open-field and found that Nav1.6<sup>cKO</sup> animals traveled significantly less distance  
144 (Fig. 1D) and were slower (Fig. 1E) compared to Nav1.6<sup>het</sup> and Nav1.6<sup>fl/fl</sup> animals. There were no  
145 genotype dependent differences in time spent moving (Fig. 1F), suggesting that motivation to move  
146 is not impaired in Nav1.6<sup>cKO</sup> mice. Time spent in the center was also not different between  
147 genotypes (Fig. S1, A). Furthermore, we did not observe any sex-dependent differences between  
148 genotypes (Fig. S1 B to D). Using a grip strength meter, we quantified grip force when all four



149 paws were placed on a metal grid and found that Nav1.6<sup>CKO</sup> animals had a significantly reduced  
150 grip strength compared to other genotypes (Fig. 1G). We next assessed motor coordination using  
151 the rotarod; however, the severe motor phenotype of Nav1.6<sup>CKO</sup> mice precluded their testing in this  
152 assay. We did not observe genotype dependent differences in latency to fall between Nav1.6<sup>het</sup> and  
153 Nav1.6<sup>fl/fl</sup> animals across training days (Fig. 1H) or on the final day of testing (Fig. 1I). Collectively,  
154 these data show that genetic ablation of Nav1.6 in sensory neurons leads to severe motor deficits  
155 that are distinct to those due to Nav1.1 deletion. Interestingly, we previously reported that Nav1.1  
156 was haploinsufficient in sensory neurons for motor behaviors; however, these results suggest a  
157 single copy of Nav1.6 is sufficient to drive normal motor function at the behavioral level.  
158 Nevertheless, we did observe Nav1.6 haploinsufficiency at the afferent level.

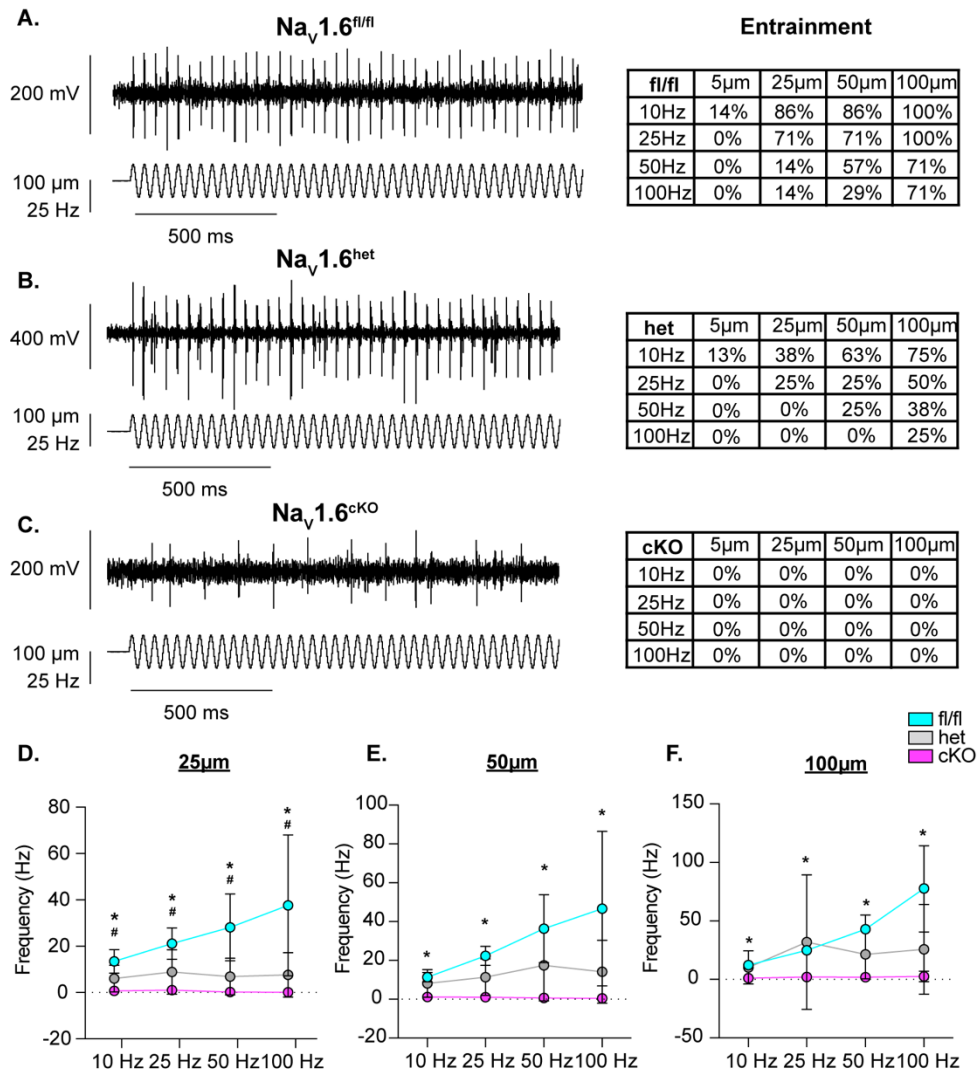


160 **Fig. 2. Loss of Nav1.6 abolishes muscle proprioceptor static stretch sensitivity.** Representative  
 161 responses to ramp-and-hold muscle stretch at 7.5% of optimal length (Lo) in  $Nav1.6^{fl/fl}$  (A),  
 162  $Nav1.6^{het}$  (B), and  $Nav1.6^{cKO}$  (C) muscle proprioceptors. The percentage of afferents that displayed  
 163 resting discharge at Lo are represented by the pie charts to the right (black indicates absence of  
 164 resting discharge). (D) Quantification of afferent firing frequency 3.25 to 3.75 seconds into stretch  
 165 protocol.  $Nav1.6^{fl/fl}$  (cyan),  $Nav1.6^{het}$  (grey), and  $Nav1.6^{cKO}$  (magenta).  $Nav1.6^{het}$  p = 0.178,  
 166  $Nav1.6^{cKO}$  p = 0.001, compared to  $Nav1.6^{fl/fl}$ . (E) Firing regularity was quantified as the coefficient  
 167 of variation of the interspike interval (ISI CV) 1.5 to 3.5 seconds into the stretch protocol.  $Nav1.6^{het}$   
 168 p = 0.669,  $Nav1.6^{cKO}$  p = 0.000, compared to  $Nav1.6^{fl/fl}$ . In 6 out of 10 animals we observed no  
 169 response to stretch and therefore could only include the quantifiable responses from 4 afferents  
 170 from  $Nav1.6^{cKO}$  mice. Only quantifiable responses were included in statistical analyses in D and E.  
 171 Box and whisker plots represent maximum, minimum, median, upper and lower quartiles of data

172 sets. Each dot represents a single afferent. A two-way mixed-design ANOVA (Dunnett's post-hoc  
173 comparison) was used to determine statistical significance in **D** and **E**. Nav1.6<sup>fl/fl</sup> n = 8, N=7;  
174 Nav1.6<sup>het</sup> n=8, N=8; Nav1.6<sup>ckO</sup> n=4, N=10. n = afferents, N = mice.

175  
176 **Nav1.6 is required for transmission of proprioceptive signals from muscle spindle afferents.**

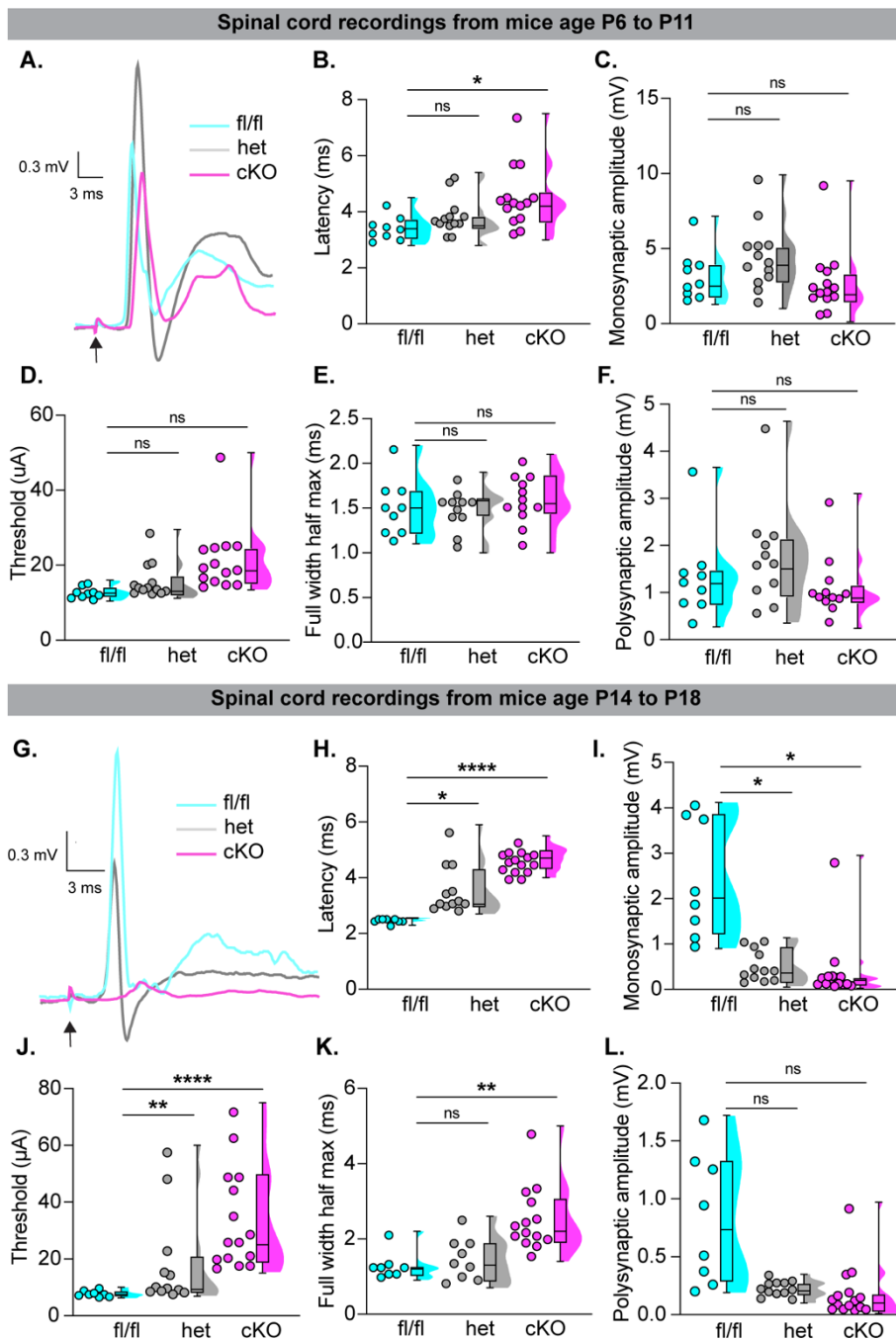
177 Our prior work found that Nav1.1 plays a key role maintaining muscle afferent activity only during  
178 static muscle stretch (7). Deletion of Nav1.1 had no effect on muscle afferent responses to dynamic  
179 muscle movement or vibratory stimuli. To test whether Nav1.6 serves a similarly specific role in  
180 proprioceptive transmission, we used an *ex vivo* muscle nerve preparation to investigate  
181 proprioceptor activity from muscle spindle afferents (16). First, we tested afferent firing in response  
182 to a series of ramp and hold stretches (Fig. 2). Afferents from Nav1.6<sup>fl/fl</sup> mice displayed consistent  
183 firing throughout the duration of a 4 s ramp and hold stretch protocol and had a high likelihood of  
184 resting discharge (Fig. 2A), consistent with wild-type Group Ia and II proprioceptor responses.  
185 Afferents from Nav1.6<sup>het</sup> mice had a similar prevalence of resting discharge compared to Nav1.6<sup>fl/fl</sup>  
186 mice and did not exhibit any significant differences in firing during ramp and hold stretches (Fig.  
187 2B). Strikingly, afferents from Nav1.6<sup>ckO</sup> mice never possessed resting discharge and  
188 neurotransmission during ramp and hold stretches were nearly abolished (Fig. 2C). In 6 out of the  
189 10 mice tested, no stretch-sensitive electrical activity was observed despite the muscle exhibiting  
190 healthy twitch contractions. We quantified afferent properties by examining instantaneous firing  
191 frequencies and found a significant reduction in firing in Nav1.6<sup>ckO</sup> afferents compared to Nav1.6<sup>fl/fl</sup>  
192 afferents across all stretch lengths (Fig. 2D). There were no significant genotype dependent  
193 differences in firing between Nav1.6<sup>het</sup> and Nav1.6<sup>fl/fl</sup> afferents. We also quantified the regularity  
194 of afferent firing by measuring the coefficient of variation of the interspike interval (ISI CV). ISI  
195 CV was similar between Nav1.6<sup>fl/fl</sup> and Nav1.6<sup>het</sup> afferents but was significantly higher in Nav1.6<sup>ckO</sup>  
196 afferents (Fig. 2E). Together these findings provide strong evidence that Nav1.6 is required for  
197 proprioceptor encoding of static stretch.



199 **Fig 3. Nav1.6 is required for proprioceptor responses to vibration.** Representative traces from  
 200 Nav1.6<sup>fl/fl</sup> (A), Nav1.6<sup>het</sup> (B), and Nav1.6<sup>cKO</sup> (C) afferents that were able to entrain to a 25 Hz, 100  
 201 μm amplitude vibration stimulus. Tables to the right indicate the percentage of afferents that were  
 202 able to entrain across stimulus frequencies and amplitudes (Nav1.6<sup>fl/fl</sup>, top; Nav1.6<sup>het</sup>, middle;  
 203 Nav1.6<sup>cKO</sup>, bottom; **D to E**) Quantification of firing frequency across vibration amplitudes. At  
 204 25μm (**D**) Nav1.6<sup>het</sup> p = 0.005 (# denotes significance in Nav1.6<sup>het</sup>), Nav1.6<sup>cKO</sup> p = 0.001, compared  
 205 to Nav1.6<sup>fl/fl</sup> (\* denotes significance in Nav1.6<sup>cKO</sup>). At 50μm (**E**) Nav1.6<sup>het</sup> p = 0.053, Nav1.6<sup>cKO</sup> p  
 206 = 0.002, compared to Nav1.6<sup>fl/fl</sup>. At 100μm (**F**) Nav1.6<sup>het</sup> p = 0.414, Nav1.6<sup>cKO</sup> p = 0.018 compared  
 207 to Nav1.6<sup>fl/fl</sup>. Nav1.6<sup>fl/fl</sup> (cyan), Nav1.6<sup>het</sup> (grey), and Nav1.6<sup>cKO</sup> (magenta). A two-way mixed-  
 208 design ANOVA (Dunnett's post-hoc comparison) was used to determine statistical in **D to F**. Box  
 209 and whisker plots represent maximum, minimum, median, upper and lower quartiles of data sets.  
 210 Each dot represents the average afferent response per genotype. Nav1.6<sup>fl/fl</sup> n = 8, N=7; Nav1.6<sup>het</sup>  
 211 n=8, N=8; and Nav1.6<sup>cKO</sup> n = 4, N=10. n=afferents, N=mice.

213 Given that Nav1.1 only contributes to proprioceptor afferent firing in response to static muscle  
 214 stretch, we next asked whether this was also true for Nav1.6. Afferents were tested using a series  
 215 of sinusoidal vibration protocols at varying frequencies and stimulus amplitudes. In line with the

216 absence of electrical activity during static stretch, Nav1.6 afferents were completely unable to  
217 entrain to vibratory stimuli regardless of stimulus amplitude and frequency (Fig. 3). Interestingly,  
218 logistic regression analyses of entrainment probability found that compared to Nav1.6<sup>fl/fl</sup> afferents,  
219 afferents from Nav1.6<sup>het</sup> animals were significantly less likely to entrain sinusoidal waves ( $p < 0.001$ ;  
220 Fig. 3 A and B). This analysis could not be used to assess entrainment probability in Nav1.6<sup>cKO</sup>  
221 afferents because these afferents never entrained to vibration. Consistent with logistic regression  
222 analyses, quantification of the instantaneous firing frequency at 25 $\mu$ m amplitude vibrations found  
223 significant impairments in the ability of Nav1.6<sup>het</sup> afferents to respond to vibration, consistent with  
224 the notion that Nav1.6 is partially haploinsufficient at the proprioceptor afferent level (Fig. 3D).  
225 Thus, unlike Nav1.1 which only serves a role in maintaining proprioceptor responses to static  
226 stretch, we find Nav1.6 plays a direct role in transmitting both dynamic and static muscle  
227 movement.



229 **Fig. 4. Nav1.6 plays a developmentally dependent role in proprioceptor synaptic transmission**  
 230 **in the spinal cord.** (A) Representative monosynaptic reflex responses from Nav1.6<sup>fl/fl</sup> (cyan),  
 231 Nav1.6<sup>het</sup> (grey), and Nav1.6<sup>cKO</sup> (magenta) hemicords during postnatal days 6 to 11. Quantification  
 232 of response properties. (B) Response latency, Nav1.6<sup>het</sup> p = 0.760, Nav1.6<sup>cKO</sup> p = 0.019, compared  
 233 to Nav1.6<sup>fl/fl</sup>. (C) Monosynaptic response amplitude, Nav1.6<sup>het</sup> p = 0.238, Nav1.6<sup>cKO</sup> p = 0.640,  
 234 compared to Nav1.6<sup>fl/fl</sup>. (D) Stimulus threshold, Nav1.6<sup>het</sup> p = 0.910, Nav1.6<sup>cKO</sup> p = 0.271,  
 235 compared to Nav1.6<sup>fl/fl</sup>. (E) Full width half max, Nav1.6<sup>het</sup> p = 0.999, Nav1.6<sup>cKO</sup> p = 0.929,  
 236 compared to Nav1.6<sup>fl/fl</sup>. (F) Polysynaptic response amplitude, Nav1.6<sup>het</sup> p = 0.514, Nav1.6<sup>cKO</sup> p = 0.704,  
 237 compared to Nav1.6<sup>fl/fl</sup>. (G) Representative monosynaptic reflex responses in Nav1.6<sup>fl/fl</sup> (cyan),  
 238 Nav1.6<sup>het</sup> (grey), and Nav1.6<sup>cKO</sup> (magenta) hemicords during postnatal days 14 to 18. (H) Response  
 239 latency, Nav1.6<sup>het</sup> p = 0.023, Nav1.6<sup>cKO</sup> p < 0.0001, compared to Nav1.6<sup>fl/fl</sup>. (I) Monosynaptic

240 response amplitude, Nav1.6<sup>het</sup> p = 0.037, Nav1.6<sup>ckO</sup> p = 0.018, compared to Nav1.6<sup>fl/fl</sup>. (J) Stimulus  
241 threshold, Nav1.6<sup>het</sup> p = 0.164, Nav1.6<sup>ckO</sup> p <0.0001, compared to Nav1.6<sup>fl/fl</sup>. (K) Full width half  
242 max, Nav1.6<sup>het</sup> p = 0.784, Nav1.6<sup>ckO</sup> p <0.0001, compared to Nav1.6<sup>fl/fl</sup>. (L) Polysynaptic response  
243 amplitude, Nav1.6<sup>het</sup> p = 0.143, Nav1.6<sup>ckO</sup> p = 0.092, compared to Nav1.6<sup>fl/fl</sup>. Each dot represents  
244 a single hemicord. (A to F) Nav1.6<sup>fl/fl</sup> n=9, Nav1.6<sup>het</sup> n=13, and Nav1.6<sup>ckO</sup> n=14. (G to L) Nav1.6<sup>fl/fl</sup>  
245 n=8, Nav1.6<sup>het</sup> n=12, and Nav1.6<sup>ckO</sup> n=15. N=8-15. n=hemicords, N=mice. Box and whisker plots  
246 represent maximum, minimum, median, upper and lower quartiles of data sets. A two-way mixed-  
247 design ANOVA (Tukey's post-hoc comparison) was used to determine statistical significance.  
248

## 249 **Nav1.6 is essential for proprioceptor synaptic transmission in a developmentally dependent** 250 **manner.**

251 Electrical signals initiated at proprioceptive end organs in skeletal muscle are transmitted to central  
252 circuits in the spinal cord. Specifically, proprioceptor Ia afferents directly synapse with alpha motor  
253 neurons, comprising the monosynaptic reflex response (17, 18). This spinal circuit provides a  
254 tractable model to assess proprioceptor synaptic transmission. Our current results demonstrate that  
255 Nav1.6 plays a central role in sensory transmission from muscle spindles; thus, we next asked  
256 whether the peripheral deficits we observed in *ex vivo* muscle nerve recordings are also evident in  
257 proprioceptive circuits in the spinal cord. We used an *ex vivo* hemisectioned spinal cord preparation  
258 and measured properties of the monosynaptic reflex circuit in Nav1.6<sup>fl/fl</sup>, Nav1.6<sup>het</sup>, and Nav1.6<sup>ckO</sup>  
259 mice (Fig. 4). We first analyzed responses from mice in early postnatal development (P6 to P11) as  
260 all prior work has used this age range for monosynaptic reflex analysis, largely due to technical  
261 challenges associated with increased myelination in the ventral horn as development proceeds (19).  
262 In stark contrast to our muscle-nerve recordings, monosynaptic responses were similar between  
263 genotypes at this timepoint (Fig. 4). We only observed a significant difference in response latency  
264 in Nav1.6<sup>ckO</sup> hemicords compared to Nav1.6<sup>het</sup> and Nav1.6<sup>fl/fl</sup> hemicords (Fig. 4B). No other  
265 genotype dependent differences were observed across quantified parameters (Fig. 4 C to F). These  
266 findings suggest that during early postnatal development, Nav1.6 is dispensable for proprioceptor  
267 synaptic transmission.  
268

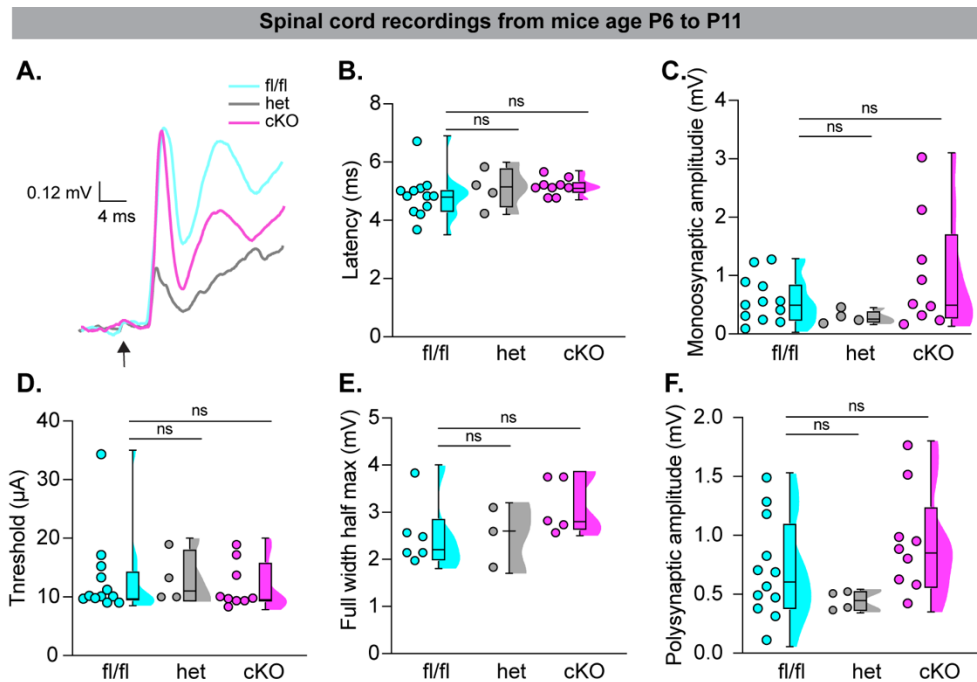
269 Interestingly, previous studies indicate that proprioceptors are not transcriptionally mature until  
270 walking behaviors begin to emerge (20), which occurs around P13. Thus, we decided to test  
271 monosynaptic responses beyond this time point (P14 to P18). To our knowledge, this is first  
272 systematic analysis of the monosynaptic reflex this late in postnatal development. Strikingly, at this  
273 age, proprioceptive synaptic transmission is nearly lost in Nav1.6<sup>cKO</sup> hemicords (Fig. 4G). We  
274 found highly significant genotype dependent differences between Nav1.6<sup>cKO</sup> and Nav1.6<sup>fl/fl</sup>  
275 hemicords across all quantified parameters (Fig. 4 H to L). This suggests that following the onset  
276 of walking behaviors, Nav1.6 is essential for proprioceptor synaptic transmission onto alpha motor  
277 neurons, which is also consistent data from *ex vivo* muscle nerve recordings in adult afferents (Figs.  
278 2 and 3). Additionally, we also found significantly increased monosynaptic reflex response  
279 latencies and thresholds (Fig. 4H and J), as well as significantly reduced response amplitudes in  
280 Nav1.6<sup>het</sup> hemicords compared to Nav1.6<sup>fl/fl</sup> controls (Fig. 4 I). Finally, when looking within  
281 genotypes, we found that unlike in Nav1.6<sup>fl/fl</sup> hemicords, which only showed a significant increase  
282 in response latency, there was a significant degradation of the monosynaptic reflex response in  
283 Nav1.6<sup>het</sup> and Nav1.6<sup>cKO</sup> hemicords (Table S1). Thus, during postnatal development, Nav1.6<sup>fl/fl</sup>  
284 animals exhibit an enhancement in central proprioceptive signaling, whereas in both Nav1.6<sup>het</sup> and  
285 Nav1.6<sup>cKO</sup> mice, central proprioceptive signaling degrades. This provides additional evidence that  
286 at the circuit level, Nav1.6 is haploinsufficient for proprioceptor synaptic function.

287  
288 The developmental dependence of the proprioceptor mediated monosynaptic reflex response on  
289 Nav1.6 prompted us to investigate motor behaviors in this line at P7 and P14, before and after the  
290 onset of weight bearing locomotion, respectively (Fig. S2). We analyzed P7 mice in a righting  
291 reflex assay, a hindlimb suspension test, a grasping reflex assay, and quantified hindlimb angle. In  
292 line with spinal cord electrophysiology data, behavioral testing at P7 found a minimal role of  
293 Nav1.6 across behavioral assays (Fig. S2, A to H); we only observed a significant difference in  
294 hindlimb angle at this age. Conversely, when we analyzed motor abilities in a limb coordination



295 assay at P14, we observed significant differences in functional grasping in both Nav1.6<sup>het</sup> and  
296 Nav1.6<sup>cKO</sup> mice compared to Nav1.6<sup>fl/fl</sup> controls (Fig. S2, I to J). These data highlight a  
297 developmentally-specific contribution of Nav1.6 to proprioceptive synaptic transmission in the  
298 spinal cord, which also manifests at the behavioral level.

299

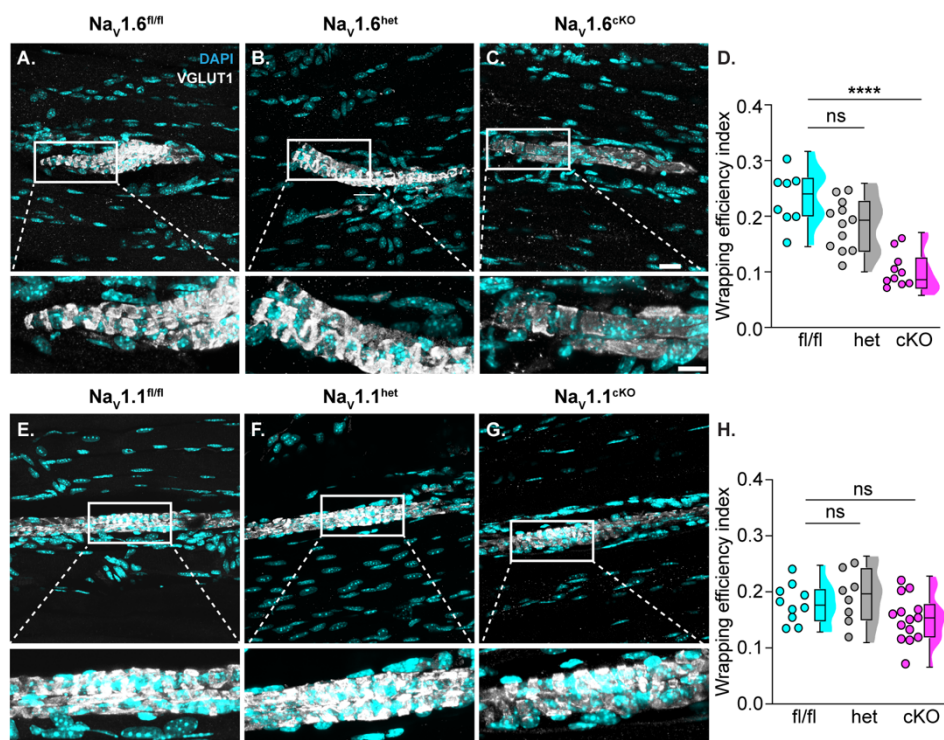


300 **Fig. 5. Nav1.1 does not contribute to proprioceptor synaptic transmission prior to the onset**  
301 **of walking behaviors.** (A) Representative monosynaptic reflex responses from Nav1.1<sup>fl/fl</sup> (cyan),  
302 Nav1.1<sup>het</sup> (grey), and Nav1.1<sup>cKO</sup> (magenta) hemicords recorded during postnatal days 6 to 11. (B to  
303 D) Quantification of monosynaptic response properties. (B) Response latency, Nav1.1<sup>het</sup> p = 0.723,  
304 Nav1.1<sup>cKO</sup> p = 0.238, compared to Nav1.1<sup>fl/fl</sup>. (C) Monosynaptic response amplitude, Nav1.1<sup>het</sup> p =  
305 0.378, Nav1.1<sup>cKO</sup> p > 0.999, compared to Nav1.1<sup>fl/fl</sup>. (D) Stimulus threshold, Nav1.1<sup>het</sup> p > 0.999 ,  
306 Nav1.1<sup>cKO</sup> p > 0.999 , compared to Nav1.1<sup>fl/fl</sup>. (E) Full width half max, Nav1.1<sup>het</sup> p > 0.999 ,  
307 Nav1.1<sup>cKO</sup> p = 0.255, compared to Nav1.1<sup>fl/fl</sup>. (F) Polysynaptic response amplitude, Nav1.1<sup>het</sup> p =  
308 0.574, Nav1.1<sup>cKO</sup> p = 0.473, compared to Nav1.1<sup>fl/fl</sup>. Each dot represents a single hemicord.  
309 Nav1.1<sup>fl/fl</sup> n=12, Nav1.1<sup>het</sup> n=4, and Nav1.1<sup>cKO</sup> n=9. N=4-10 mice. Box and whisker plots represent  
310 maximum, minimum, median, upper and lower quartiles of data sets. A Kruskal-Wallis test with  
311 Dunn's multiple comparisons was used to determine statistical significance.

312

313 Because we did not observe a role for Nav1.6 in the proprioceptor mediated monosynaptic reflex  
314 response between P6 and P11, we next asked whether instead Nav1.1 was required for  
315 proprioceptor synaptic transmission at this developmental stage. In line with our findings across  
316 Nav1.6 genotypes, monosynaptic reflex responses were genotype-independent in the Nav1.1 mouse  
317 line in this age range (Fig. 5). These data suggest that proprioceptor synaptic transmission at early

318 postnatal development is not dependent on Nav1.1 or Nav1.6 and could indicate Nav functional  
319 redundancy in proprioceptors prior to the onset of walking behaviors. We attempted to measure the  
320 monosynaptic reflex in later postnatal development (P14 to P18) in these mice; however, responses  
321 across all genotypes were too small to reliably quantify, despite our ability to obtain recordings at  
322 this age from mice in the Nav1.6-line (Fig. 4) as well as age matched C57Bl/6J controls (Fig. S3).  
323 Thus, we cannot rule out the possibility that Nav1.1 may serve a role in proprioceptor mediated  
324 synaptic transmission following the acquisition of weight bearing locomotion. Behavioral testing  
325 at P7 did not reveal changes in motor function across genotypes (Fig. S4 A to B). At P14 however,  
326 we did observe a significant difference in functional grasping in Nav1.1<sup>cKO</sup> mice compared to  
327 Nav1.1<sup>fl/fl</sup> controls (Fig. S4E), suggesting Nav1.1 is also becomes required for motor coordination  
328 at the onset of walking behaviors. These data show that in early postnatal development neither  
329 Nav1.6 or Nav1.1 alone is required for proprioceptor synaptic transmission; however, upon the  
330 acquisition of weight-bearing locomotion, we find that Nav1.6 becomes functionally dominant at  
331 the circuit level, and both Nav1.1 and Nav1.6 are required at the behavioral level.



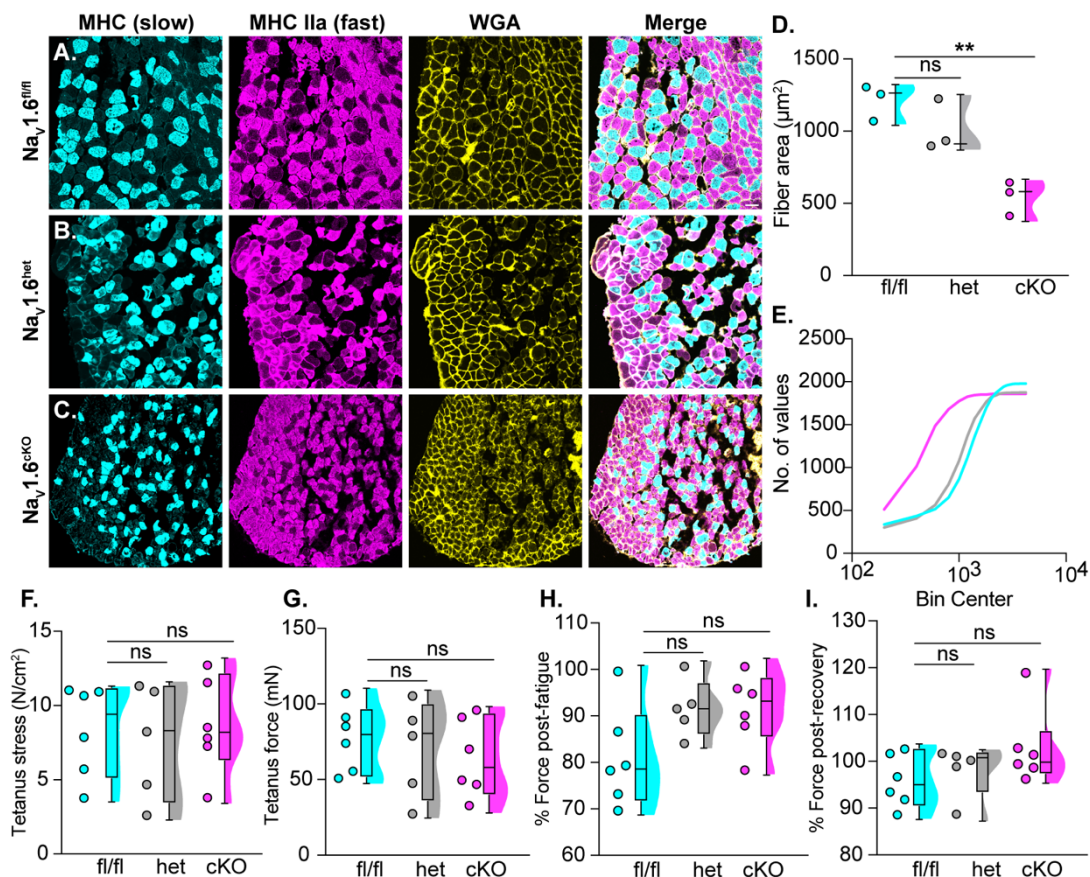
332 **Fig. 6. Electrical signaling deficits associated with Nav1.6- but not Nav1.1-deletion impairs**  
333 **muscle spindle development.** Representative confocal images of muscle spindles from (A)

334 Nav1.6<sup>fl/fl</sup>, (B) Nav1.6<sup>het</sup>, and (C) Nav1.6<sup>cKO</sup> extensor digitorum longus (EDL) muscle sections (30  
335  $\mu$ m). Images were acquired with a 60x oil 1.4 NA lens. VGLUT1 (grey scale) labels proprioceptor  
336 sensory terminals and DAPI (cyan) labels nuclei. Insets below images show the colocalization of  
337 sensory terminals with DAPI. (D) Quantification of wrapping efficiency index based on  
338 colocalization of DAPI with VGLUT1. Nav1.6<sup>het</sup>  $p = 0.0658$ , and Nav1.6<sup>cKO</sup>,  $p < 0.0001$ , compared  
339 to Nav1.6<sup>fl/fl</sup>. Representative images of muscle spindles from (E) Nav1.1<sup>fl/fl</sup>, (F) Nav1.1<sup>het</sup>, (G)  
340 Nav1.1<sup>cKO</sup>. (H) Quantification of wrapping efficiency index based on colocalization of DAPI with  
341 VGLUT1. Nav1.1<sup>het</sup>,  $p = 0.762$ , and Nav1.1<sup>cKO</sup>,  $p = 0.282$ , compared to Nav1.1<sup>fl/fl</sup>. Each dot  
342 represents a single muscle spindle section. (D) Nav1.6<sup>fl/fl</sup>  $n=8$ , Nav1.6<sup>het</sup>  $n=12$ , and Nav1.6<sup>cKO</sup>  $n=10$ .  
343 (H) Nav1.1<sup>fl/fl</sup>  $n=10$ , Nav1.1<sup>het</sup>  $n=8$ , and Nav1.1<sup>cKO</sup>  $n=14$ .  $N=3$  mice per genotype. Box and whisker  
344 plots represent maximum, minimum, median, upper and lower quartiles of data sets. A one-way  
345 ANOVA (Dunnett's post-hoc comparison) was used to determine statistical significance. Scale bar  
346 = 20  $\mu$ m. Inset scale bar = 10  $\mu$ m.

347  
348 **Severely, but not moderately, impaired proprioception results in deficits in muscle spindle**  
349 **development.**

350 A recent study found that loss of Piezo2 or Nav1.6 in sensory neurons led to changes in tactile  
351 sensory neuron end organ development (21). This study raised the possibility that Nav1.6 may also  
352 regulate muscle spindle development. As with our prior examination of Nav1.1<sup>cKO</sup> mice compared  
353 to controls, we did not observe a reduction in the overall number of proprioceptors in DRG sections  
354 (identified by *Pvalb* and *Runx3* colocalization) between Nav1.6<sup>fl/fl</sup>, Nav1.6<sup>het</sup>, and Nav1.6<sup>cKO</sup> mice  
355 (Fig. S5 B). We next examined the structure of muscle spindles in Nav1.6<sup>cKO</sup> mice by performing  
356 immunohistochemistry against vesicular glutamate transporter 1 (VGLUT1) to visualize muscle  
357 spindle sensory wrappings in sections of extensor digitorum longus muscle. Qualitative observation  
358 of muscle spindles from Nav1.6<sup>cKO</sup> mice show striking structural abnormalities in sensory  
359 wrappings that were not present in Nav1.6<sup>fl/fl</sup> or Nav1.6<sup>het</sup> animals (Fig. 6 A to C). To validate that  
360 the structural changes we observed were not due disruptions in VGLUT1 expression, a subset of  
361 experiments were conducted with both VGLUT1 and the pan-neuronal marker  $\beta$ III-tubulin. Both  
362 antibodies showed highly similar levels of immunoreactivity, indicating VGLUT1 is a good proxy  
363 for muscle spindle structure (Fig. S6). To our knowledge there is no standardized method to  
364 quantitatively assess the structure of muscle spindles. Thus, we devised a quantitative method to  
365 examine muscle spindle sensory terminals by measuring the colocalization of VGLUT1<sup>+</sup> sensory

366 wrappings around clusters of DAPI-positive nuclei, which represent intrafusal muscle fibers. By  
 367 normalizing the number of wrappings to muscle spindle length, we calculated a wrapping efficiency  
 368 index. We found that compared to Nav1.6<sup>fl/fl</sup> and Nav1.6<sup>het</sup> animals, muscle spindles from  
 369 Nav1.6<sup>cKO</sup> mice had significantly reduced wrapping efficiency indices, demonstrating that Nav1.6  
 370 in sensory neurons is required for muscle spindle development (Fig. 6D). In our prior work, we  
 371 qualitatively reported that loss of Nav1.1 does not change muscle spindle structure (7). To confirm  
 372 our previous findings using this quantitative approach, we analyzed the wrapping efficiency index  
 373 of muscle spindles from Nav1.1<sup>cKO</sup> mice compared to Nav1.1<sup>het</sup> and Nav1.1<sup>fl/fl</sup> controls (Fig. 6 E to  
 374 H). In line with our previous work, Nav1.1 is not required for muscle spindle development as  
 375 wrapping efficiency indices were not significantly different between genotypes (Fig. 6H). Thus, the  
 376 above results show that muscle spindle development is impaired when proprioceptive signaling is  
 377 severely, but not moderately, disrupted.



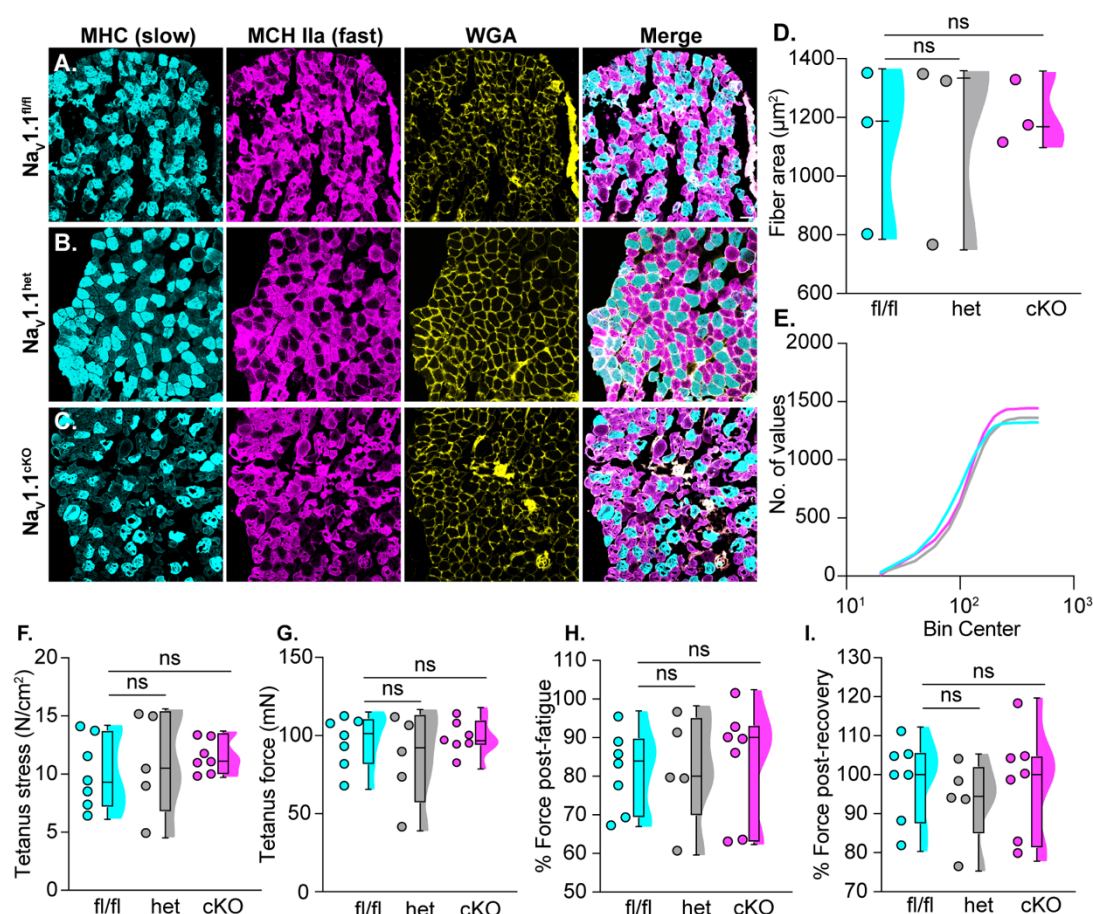
378

379 **Fig 7. Loss of proprioceptive feedback alters skeletal muscle development in Nav1.6<sup>CKO</sup> mice.**  
380 Representative images of muscle fibers from the soleus of (A) Nav1.6<sup>fl/fl</sup>, (B) Nav1.6<sup>het</sup>, and (C)  
381 Nav1.6<sup>CKO</sup> mice. Images were acquired with a 20x 0.75 NA air lens. Myosin heavy chain (MHC),  
382 labels slow twitch muscle fibers (cyan), MHC type IIa labels fast twitch muscle fibers (magenta),  
383 and wheat germ agglutinin (WGA, yellow) labels the cell membrane of muscle fibers. (D and E)  
384 Quantification of muscle fiber anatomy. (D) Fiber area, Nav1.6<sup>het</sup> p = 0.337, Nav1.6<sup>CKO</sup> p = 0.006,  
385 compared to Nav1.6<sup>fl/fl</sup>. (E) cumulative distribution plots showing the muscle fiber area in the soleus  
386 between Nav1.6<sup>fl/fl</sup> (cyan), Nav1.6<sup>het</sup> (grey), and Nav1.6<sup>CKO</sup> (magenta) mice. (F to I) Quantification  
387 of intrinsic properties of soleus muscle. (F) Tetanus stress, Nav1.6<sup>het</sup> p = 0.926, Nav1.6<sup>CKO</sup> p =  
388 0.990, compared to Nav1.6<sup>fl/fl</sup>. (G) Tetanus force, Nav1.6<sup>het</sup> p = 0.925, Nav1.6<sup>CKO</sup> p = 0.690,  
389 compared to Nav1.6<sup>fl/fl</sup>. (H) Percentage of force post-fatigue, Nav1.6<sup>het</sup> p = 0.189, Nav1.6<sup>CKO</sup> p =  
390 0.150, compared to Nav1.6<sup>fl/fl</sup>. (I) Percentage of force post-recovery, Nav1.6<sup>het</sup> p = 0.851, Nav1.6<sup>CKO</sup>  
391 p = 0.293, compared to Nav1.6<sup>fl/fl</sup>. Each dot represents a single animal. Box and whisker plots  
392 represent maximum, minimum, median, upper and lower quartiles of data sets. A one-way ANOVA  
393 (Dunnnett's post-hoc comparison) was used to determine statistical significance. Scale bar=50  $\mu$ m.

### 395 **Proprioceptive feedback is required for normal skeletal muscle development.**

396 Global inactivation of Nav1.6 leads to severe motor impairments accompanied by atrophy of  
397 skeletal muscle (22). It was hypothesized that these deficits were caused by loss of signal  
398 transmission from motor neurons; however, whether impaired proprioceptive feedback onto motor  
399 neurons is sufficient to impair skeletal muscle development has not been directly investigated. To  
400 address this, we analyzed skeletal muscle anatomy and function in the Nav1.6 mouse line. We  
401 collected soleus muscle from mice and labeled for slow (Type I) and fast (Type IIa) twitch muscle  
402 fibers. Muscle fibers from Nav1.6<sup>CKO</sup> mice had a visible reduction in muscle fiber size compared to  
403 fibers from Nav1.6<sup>het</sup> and Nav1.6<sup>fl/fl</sup> mice (Fig. 7 A to C). To quantify these changes, we took an  
404 unbiased approach and measured muscle fiber properties using a semi-automatic muscle fiber  
405 analysis software in MATLAB (23). In agreement with qualitative observation, muscle fibers from  
406 Nav1.6<sup>CKO</sup> mice displayed a significant decrease in fiber area compared to Nav1.6<sup>het</sup> and Nav1.6<sup>fl/fl</sup>  
407 muscle (Fig. 7 D). A cumulative distribution plot shows the spread of muscle fiber area across  
408 genotypes (Fig. 7E). The proportion of Type I and Type IIa fibers were also similar between  
409 genotypes and were within the expected percentages for soleus muscle in wildtype animals (Fig.  
410 S7 A and B, 24, 25). Furthermore, we found that the size of both Type I and Type IIa fibers in  
411 Nav1.6<sup>CKO</sup> mice were significantly reduced compared to other genotypes, indicating the changes in

412 muscle fiber diameter and area were not fiber-type specific (Fig S7 C and D). We next examined  
 413 whether the developmental changes in muscle fiber properties corresponded to alterations in  
 414 intrinsic muscle strength and fatiguability; however, we found no differences in muscle function  
 415 across genotypes (Fig. 7 F to I). Collectively, these reveal a non-cell autonomous role for  
 416 proprioceptive feedback in skeletal muscle development.  
 417

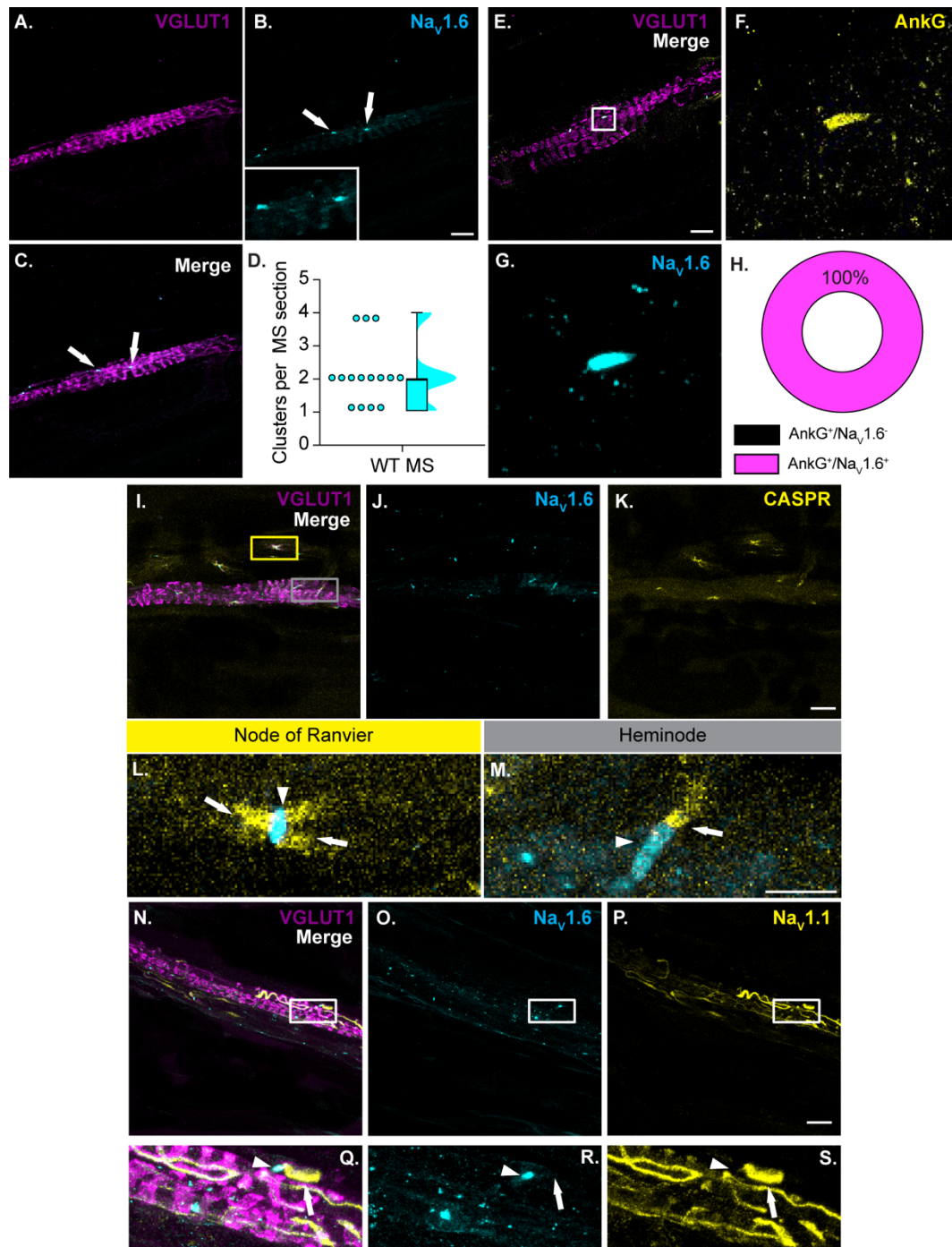


418 **Fig. 8. Mildly impaired proprioceptive feedback does not impair skeletal muscle development.**  
 419 Images of muscle fibers from (A)  $Nav1.1^{fl/fl}$ , (B)  $Nav1.1^{het}$ , and (C)  $Nav1.6^{cKO}$  soleus muscle.  
 420 Images were acquired with a 20x 0.75 NA air lens. Myosin heavy chain (MHC) labels slow twitch  
 421 muscle fibers (cyan), MHC type IIa labels fast twitch muscle fibers (magenta), and wheat germ  
 422 agglutinin (WGA, yellow) labels the cell membrane of muscle fibers. (D and E) Quantification of  
 423 muscle fiber anatomy. (D) Fiber area,  $Nav1.1^{het}$   $p = 0.9827$ ,  $Nav1.1^{cKO}$   $p = 0.880$ , compared to  
 424  $Nav1.1^{fl/fl}$ . (E) cumulative distribution plots showing the muscle fiber area between  $Nav1.1^{fl/fl}$   
 425 (cyan),  $Nav1.1^{het}$  (grey), and  $Nav1.1^{cKO}$  (magenta). (F to I) Quantification of intrinsic properties of  
 426 soleus muscle. (F) Tetanus stress,  $Nav1.1^{het}$   $p = 0.841$ ,  $Nav1.1^{cKO}$   $p = 0.596$ , compared to  $Nav1.1^{fl/fl}$ .  
 427 (G) Tetanus force,  $Nav1.1^{het}$   $p = 0.624$ ,  $Nav1.1^{cKO}$   $p = 0.978$ , compared to  $Nav1.1^{fl/fl}$ . (H)  
 428 Percentage of force post-fatigue,  $Nav1.1^{het}$   $p = 0.999$ ,  $Nav1.1^{cKO}$   $p = 0.934$ , compared to  $Nav1.1^{fl/fl}$ .  
 429 (I) Percentage of force post-recovery,  $Nav1.1^{het}$   $p = 0.724$ ,  $Nav1.1^{cKO}$   $p = 0.993$ , compared to  
 430  $Nav1.1^{fl/fl}$ . Each dot represents a single animal. Box and whisker plots represent maximum,

431 minimum, median, upper and lower quartiles of data sets. A one-way ANOVA (Dunnett's post-hoc  
432 comparison) was used to determine statistical significance. Scale bar=50  $\mu\text{m}$ .

433

434 We next asked whether moderately impaired proprioceptive signaling due to loss of Nav1.1 had the  
435 same effect on skeletal muscle development or function. We examined muscle fiber composition  
436 of Nav1.1 mice of all genotypes and did not observe any significant changes in fiber area (Fig. 8 A  
437 to E). Additionally, the proportion of Type I and Type IIa fibers were similar between genotypes  
438 (Fig. S7 E to F). Functional analysis of intrinsic muscle properties in the soleus of Nav1.1<sup>cKO</sup> mice  
439 did not differ compared to Nav1.1<sup>het</sup> or Nav1.1<sup>fl/fl</sup> mice (Fig. 8 F to I), suggesting moderately  
440 impaired proprioceptive feedback does not result in deficits in skeletal muscle developmental at the  
441 anatomical or functional levels. Taken together, these experiments unveil a novel role for  
442 proprioceptive feedback in skeletal muscle development.



444 **Fig 9. Nav1.1 and Nav1.6 localize to discrete cellular regions in muscle spindles.** VGLUT1  
445 (magenta, A) labeled muscle spindles express clusters of Nav1.6 (cyan, B and C). Arrows denote  
446 clusters of Nav1.6. (D) Quantification of the number of Nav1.6 clusters per muscle spindle (n=15  
447 spindles). (E to H) Nav1.6 clusters (G) colocalize with Ankyrin-G (yellow, E and F are insets from  
448 G). (H) Quantification of the percentage of Ankyrin G clusters that colocalize with Nav1.6 clusters  
449 (n=9 spindles). (I to M) Co-labeling of Nav1.6 (J) with juxtaparanode maker CASPR (K, yellow)  
450 reveal proprioceptor nodes of Ranvier (L) and heminodes (M) (n=10 spindles). Nodes of Ranvier  
451 were identified by two CASPR<sup>+</sup> signals (arrows) flanking Nav1.6 clusters (arrowhead). Heminodes  
452 were identified by a single CASPR<sup>+</sup> signals juxtaposed to Nav1.6 cluster. (N to S) Co-labeling of  
453 Nav1.6 (O) with Nav1.1 (P, yellow) show discrete cellular expression patterns. (Q to S) Arrowhead



454 denotes Nav1.6 channels and arrows denote Nav1.1 channels. N=3-5 mice. Inset scale bars=10  $\mu$ m.  
455 Scale bars=20  $\mu$ m  
456

### 457 **Nav1.1 and Nav1.6 occupy distinct cellular domains within muscle spindles**

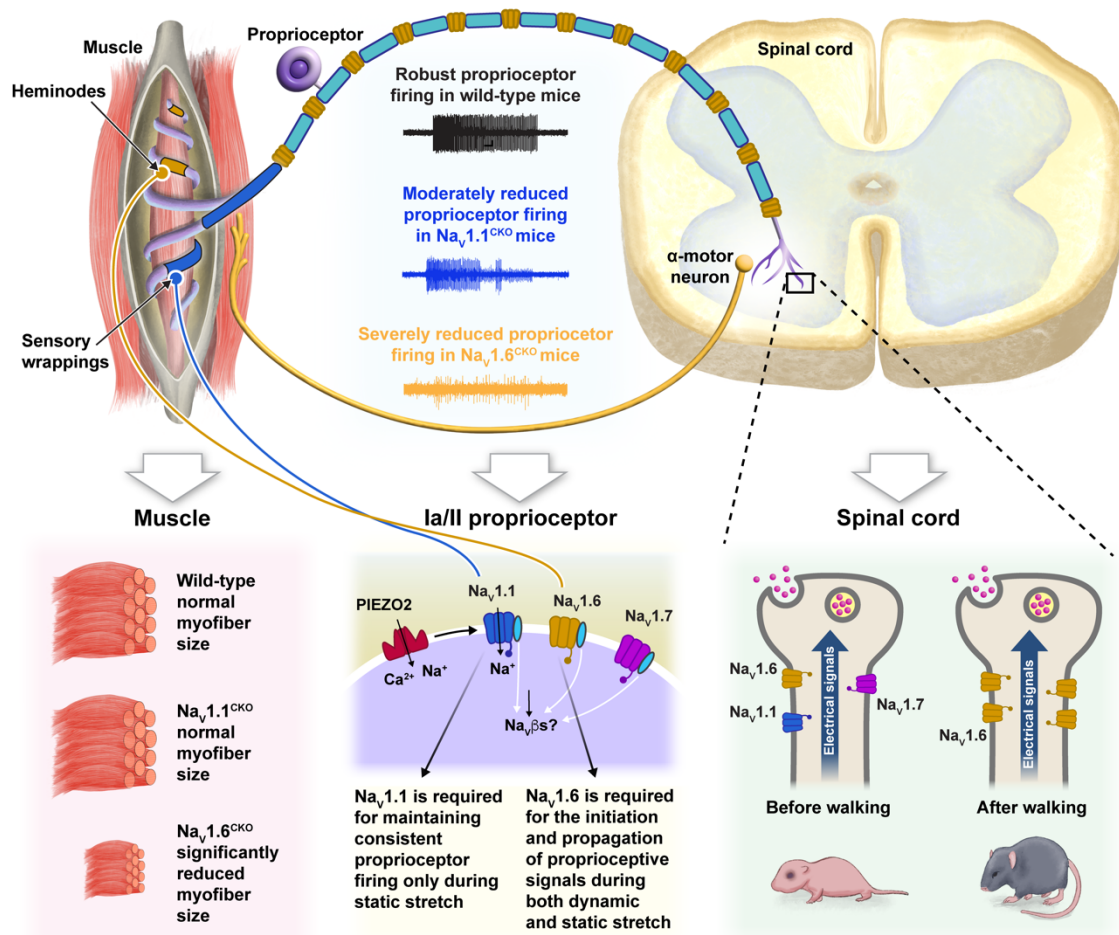
458 Our results demonstrate that Nav1.1 and Nav1.6 have differential roles in proprioceptive signaling.  
459 We next sought out to define the mechanistic basis of their distinct and nonredundant contributions.  
460 At the biophysical level, Nav1.1 and Nav1.6 are functionally very similar, and both contribute to  
461 peak, persistent, and resurgent sodium currents (26–28). Previous studies examining central  
462 neurons, however, show that Nav1.1 and Nav1.6 occupy distinct excitable domains (29–31),  
463 suggesting that differences in cellular localization could dictate the unique roles these channels play  
464 in proprioception. Compared to the central nervous system, our understanding of Nav expression  
465 in sensory terminals is extremely poor. We therefore set out to examine the expression patterns of  
466 Nav1.1 and Nav1.6 in proprioceptive end organs. We focused our analysis on muscle spindles, as  
467 these structures comprise two of the three proprioceptor functional classes (1) and are the afferent  
468 endings from which we recorded in *ex vivo* muscle nerve experiments (Figs. 2 and 3). We first  
469 labeled for Nav1.6 channels and observed discrete, high density clusters across the spindle that  
470 resembled action potential initiation zones (Fig. 9A to C). We observed approximately 2 Nav1.6<sup>+</sup>  
471 clusters per muscle spindle section (Fig. 9D), though this is likely an underestimation of the total  
472 number of clusters per entire spindle. In central neurons, Nav1.6 has been shown to play a major  
473 role in signal initiation and propagation due to its expression at the distal axon initial segment (AIS)  
474 and nodes of Ranvier (29, 31, 32). Thus, we co-labeled with the AIS marker Ankyrin-G (AnkG,  
475 Fig. 9 E to G, 33) and found that 100% of Nav1.6 clusters colocalize with AnkG (Fig. 9 H). To  
476 determine if these clusters were *bona fide* heminodes or nodes of Ranvier, we co-labeled with the  
477 juxtaparanode marker CASPR (34). Indeed, triple immunolabelling experiments found Nav1.6  
478 clusters flanked by two CASPR<sup>+</sup> signals near VGLUT1<sup>+</sup> muscle spindles (Fig. 9 I to L), as well as  
479 in myelinated axons of the sciatic nerve (Fig. S8). Furthermore, we also observed Nav1.6 channel

480 clusters flanked by a single CASPR<sup>+</sup> signal within muscle spindles, indicative of the presence of  
481 Nav<sub>v</sub>1.6<sup>+</sup> heminodes (Fig. 9 M). We ensured the specificity of Nav<sub>v</sub>1.1 and Nav<sub>v</sub>1.6 antibodies using  
482 tissue harvested from Nav<sub>v</sub>1.1<sup>ckO</sup> and Nav<sub>v</sub>1.6<sup>ckO</sup> mice, respectively (Fig. S9). These findings reveal  
483 that Nav<sub>v</sub>1.6 is expressed only at heminodes within muscle spindles and nodes of Ranvier of  
484 proprioceptors, where it likely plays a direct role in signal initiation and propagation.

485  
486 If Nav<sub>v</sub>1.1 and Nav<sub>v</sub>1.6 differentially regulate electrical signaling in proprioceptors through distinct  
487 cellular localization patterns, co-labeling for both ion channels should reveal non-overlapping  
488 expression patterns. In line with our hypothesis, we find a notable difference in Nav<sub>v</sub>1.1 localization  
489 in muscle spindles compared to Nav<sub>v</sub>1.6 (Fig 9 N and Q). In contrast to the discrete clusters of  
490 Nav<sub>v</sub>1.6, we observe Nav<sub>v</sub>1.1 localization is broader, but restricted to more equatorial wrappings  
491 within muscle spindles and in some presumptive axons entering the muscle spindle (Fig. 9 S).

492  
493 Given we found developmentally dependent roles for Nav<sub>v</sub>1.1 and Nav<sub>v</sub>1.6 in proprioceptor synaptic  
494 transmission in the spinal cord (Figs. 4 and 5), we asked whether Nav<sub>v</sub> localization is dynamic during  
495 postnatal development. We labeled for Nav<sub>v</sub>1.1 and Nav<sub>v</sub>1.6 in muscle spindles from the EDL of P7  
496 and P14 C57Bl6/J mice (Fig. S10), the timepoints at which we observed a change in the requirement  
497 for either channel to motor function (Figs. S2 and S4). At P7, we observed no Nav<sub>v</sub>1.6 clusters within  
498 spindles, though we did find some clusters near spindles, which could represent nodes of Ranvier.  
499 At P14, clusters of Nav<sub>v</sub>1.6 begin to emerge within muscle spindles, though these clusters appear  
500 smaller and less frequently than those observed in adult muscle spindles. We detected little to no  
501 Nav<sub>v</sub>1.1 immunoreactivity in muscle spindles at P7 and P14, suggesting either no or low expression  
502 of this channel at these timepoints. Given the significant change in functional grasping observed in  
503 Nav<sub>v</sub>1.1<sup>ckO</sup> at P14 (Fig. S4E) this would suggest Nav<sub>v</sub>1.1 may serve a role in sensory transmission  
504 outside of the muscle spindle at this timepoint in postnatal development. Thus, we propose that the

505 unique localization patterns of Nav1.1 and Nav1.6, which are dynamically regulated during  
 506 postnatal development, confer the unique contributions of each channel to electrical signaling in  
 507 proprioceptors.



508  
 509 **Fig. 10. Model of proprioceptive transmission by Nav1.1 and Nav1.6.** Upon muscle stretch,  
 510 Piezo2 (red) transduces mechanical stimuli into electrical potentials. Following Piezo2 activation,  
 511 Nav1.1 (blue) expressed in muscle spindle sensory terminals drives consistent proprioceptor firing  
 512 during static muscle stretch. Nav1.6 (yellow) localized to heminodes and nodes of Ranvier initiate  
 513 and propagate all proprioceptive signals from muscle spindles to spinal cord. It is likely prior to  
 514 walking, there is functional redundancy of Navs in proprioceptive axons. After walking behaviors  
 515 emerge however, proprioceptive synaptic transmission is dependent on Nav1.6. Deletion of Nav1.6  
 516 in all sensory neurons led to a significant decrease in skeletal muscle fiber size that was not present  
 517 in Nav1.1<sup>cKO</sup> muscle, suggesting that complete loss of proprioceptive feedback non-cell  
 518 autonomously regulates skeletal muscle development.

519  
 520

## 521 Discussion

522

523 The discovery of Piezo2 shared the 2021 Nobel Prize in Physiology and Medicine due to its  
524 essential role in the function of various mechanosensory neurons. In proprioceptors, Piezo2 initiates  
525 muscle mechanotransduction signaling (4, 5); however, the downstream ion channels responsible  
526 for transmitting proprioceptive information to central circuits has remained mysterious. Here, we  
527 demonstrate that Navs differentially encode mammalian proprioception, and we predict this is  
528 largely due to differences in channel localization within proprioceptors (Fig. 10). Our prior work  
529 found that Nav1.1 is essential for maintaining consistent and reliable proprioceptor encoding of  
530 static muscle stretch (7); this is consistent with its expression at sensory wrappings of muscle  
531 spindles where it is poised to amplify Piezo2-mediated mechanotransduction currents. Conversely,  
532 due to its localization at heminodes within muscle spindles and nodes of Ranvier, Nav1.6 has an  
533 obligate role in initiating proprioceptor action potential firing. This is in line with *ex vivo* recordings  
534 from Nav1.6<sup>CKO</sup> afferents, in which responses to both dynamic and static muscle movement are  
535 abolished (Figs. 2 and 3). Furthermore, this demonstrates that the activity of Piezo2 and other ion  
536 channels in proprioceptors cannot compensate for the loss of Nav1.6. Thus, we conclude that  
537 Nav1.6 is equally essential for mammalian proprioception as Piezo2. To our knowledge, this is the  
538 first study to investigate and define unique and nonredundant roles for Navs in somatosensory  
539 encoding.

540

541 At the behavioral level, deletion of Nav1.1 or Nav1.6 in sensory neurons led to phenotypically  
542 distinct motor deficits. Previously, we reported that Nav1.1<sup>CKO</sup> mice display uncontrollable  
543 intention-like tremors and poor motor coordination (7). Here we show that deletion of Nav1.6 in  
544 sensory neurons resulted in even more severe ataxia that precluded testing in the rotarod (Fig. 1).  
545 Notably, though more impaired than Nav1.1<sup>CKO</sup> mice, Nav1.6<sup>CKO</sup> mice did not display intention  
546 tremors. The distinct motor phenotypes that result from conditional deletion of Nav1.1 or Nav1.6

547 likely arise from differences in their respective contributions to proprioceptor function and  
548 development (Figs. 2, 3 and 6). It should be noted, however, that the behavioral phenotypes in these  
549 models cannot solely be attributed to proprioceptor dysfunction, as Nav1.1 and Nav1.6 are also  
550 expressed in tactile sensory neurons (35), which also contribute to motor behaviors (36, 37).  
551 Nevertheless, at the afferent level, we show Nav1.6 is fundamentally essential for electrical  
552 signaling in proprioceptors, which contrasts the selective impairment on static stretch encoding  
553 observed in Nav1.1<sup>CKO</sup> mice. Furthermore, Nav1.1 deletion had no significant impact on muscle  
554 spindle or skeletal muscle development; therefore, it is likely that the deficits observed in Nav1.1<sup>CKO</sup>  
555 are purely electrical in nature. By contrast, in addition to loss of proprioceptive transmission,  
556 Nav1.6<sup>CKO</sup> mice had abnormal muscle spindle structure (Fig. 6) and significantly reduced skeletal  
557 muscle fiber size (Fig. 7), which suggests that the severe motor deficits in Nav1.6<sup>CKO</sup> may be caused  
558 by both cell-autonomous and non-cell-autonomous mechanisms. Interestingly, prior work on  
559 *Scn8a*<sup>med</sup> mice show that global inactivation of Nav1.6 resulted in a similar ataxic-like phenotype,  
560 as well as muscle atrophy and weakness (12, 22). Our data show loss of Nav1.6 function in sensory  
561 neurons, particularly proprioceptors, are a major contributor to the motor and muscle impairments  
562 in *Scn8a*<sup>med</sup> mice. This may have broader implications for interpreting the clinical manifestations  
563 associated with disease causing *Scn8a* mutations, which often result in motor dysfunction (11).

564  
565 We found that a single copy of Nav1.6 in sensory neurons was sufficient for normal motor function  
566 in adults (Fig. 1), despite being haploinsufficient in *ex vivo* muscle nerve recordings in response to  
567 vibration (Figs. 3). Indeed, in response to vibratory stimuli, afferents from Nav1.6<sup>het</sup> animals were  
568 less likely to entrain to sinusoidal vibration, particularly at 25 $\mu$ m stimulus amplitudes (Fig. 3 B and  
569 D). Why these functional deficits in Nav1.6<sup>het</sup> afferents do not manifest at the behavioral level is  
570 unclear. It should be noted that at P14 we observed Nav1.6 haploinsufficiency in *ex vivo*  
571 monosynaptic reflex recordings (Fig. 4 and Table S1) and in a motor coordination assay (Fig S2).

572 It is therefore possible that compensatory mechanisms in Nav1.6<sup>het</sup> animals come into play in early  
573 adulthood. Another possibility is that Nav1.6<sup>het</sup> animals possess more subtle motor deficits that  
574 were unresolvable in the open field and rotarod. More sensitive kinematic analyses with higher  
575 spatial and temporal resolution will be required to investigate the extent of Nav1.6  
576 haploinsufficiency for proprioceptor-driven motor behaviors.

577

578 We have very limited knowledge about the localization of ion channels within somatosensory end  
579 organs. This information is important for understanding how electrical signals arise within  
580 structurally complex sensory terminals, which can be damaged during pathological conditions or  
581 aging (1, 38–40). We show that Nav1.1 and Nav1.6 occupy distinct cellular compartments within  
582 proprioceptive muscle spindle end organs, which we predict underlies their differential roles in  
583 encoding proprioceptive signals. While differences in biophysical properties could also underly the  
584 differential roles of Nav1.1 and Nav1.6 to proprioceptive transmission, these channels share many  
585 functional similarities. They both rapidly activate and inactivate, can generate peak, persistent and  
586 resurgent currents, and have similar recovery from inactivation kinetics (7, 27, 28, 41–43). Prior  
587 work in neurons of the central nervous system is consistent with our hypothesis that localization  
588 dictates Nav contributions to proprioceptor function. For example, in retinal ganglion cells and  
589 motor neurons, Nav1.6 is preferentially expressed at the distal axon initial segment, suggesting a  
590 primary role in signal initiation (44, 45). Furthermore, studies have shown that Nav1.6 is the  
591 dominant isoform at nodes of Ranvier, playing a key role in action potential propagation in  
592 myelinated axons (31, 45). In contrast, Nav1.1 is localized to the soma and proximal AIS, where it  
593 aids in repetitive firing in fast spiking neurons of the brain (14, 46). This is in line with our model  
594 whereby Nav1.1 amplifies mechanotransduction currents from Piezo2 to maintain sustained action  
595 potential firing during static stretch.

596

597 Interestingly, we found that 100% of Nav1.6 immunoreactivity colocalizes with AnkG. AnkG is  
598 known to anchor Navs within the AIS of central neurons (32, 33, 47, 48); thus, our findings indicate  
599 muscle spindles possess several Nav1.6-expressing action potential initiation zones. Surprisingly,  
600 we never observed broad AnkG immunoreactivity in muscle spindle sensory wrappings, indicating  
601 AnkG does not colocalize with Nav1.1, despite its known colocalization with Nav1.1 at the AIS in  
602 other neurons of the central nervous system (30, 49). The mechanisms that anchor Nav1.1 to  
603 sensory terminals remain unknown. Scaffolding proteins known to colocalize with Nav1.1 include  
604  $\beta$ IV-spectrin, auxiliary Nav $\beta$  subunits, and fibroblast growth factors (14, 50, 51). Proximity  
605 proteomic approaches could identify specific molecular players involved in Nav1.1 channel  
606 organization within proprioceptive end organs.

607

608 Another surprising result from our study was the developmentally dependent manner in which Navs  
609 contribute to proprioceptor synaptic transmission in the spinal cord (Fig. 10). Ventral root  
610 recordings from mice at ages P6 to P11 revealed that neither Nav1.1 or Nav1.6 are required for the  
611 proprioceptor-mediated monosynaptic reflex response at this age. Conversely, by P14, when  
612 proprioceptors are nearing molecular maturation and weight bearing locomotion has emerged,  
613 Nav1.6 becomes absolutely critical for this circuit. There are two principal interpretations for these  
614 data. First, prior to walking behaviors, neither Nav1.1 or Nav1.6 contribute to proprioceptor  
615 synaptic transmission onto motor neurons. This interpretation would be consistent with previous  
616 studies in myelinated neurons of the retina, whereby the onset of eye opening corresponds with a  
617 developmental switch from Nav1.2 to Nav1.6 (44). It is possible that another Nav subtype, such as  
618 Nav1.7, is the dominant channel in early postnatal development. Alternatively, another  
619 interpretation is that in early postnatal development, there is functional redundancy among Nav  
620 subtypes, and loss of one is insufficient to impair synaptic transmission. This is line with a previous  
621 study that found the presence of multiple Nav isoforms in sensory axons as early as P7 (52). We

622 favor the latter interpretation because functional redundancy is a common phenomenon in the  
623 developing nervous system, and Nav1.7 does not appear to play a significant role in mammalian  
624 proprioception. Nevertheless, both interpretations indicate that the cellular trafficking mechanisms  
625 governing the stability of each Nav subtype in this circuit are independent of one another, as loss  
626 of Nav1.6 did not result in compensation by other Navs following the onset of weight bearing  
627 locomotion. Notably, our analyses of the monosynaptic reflex are consistent with behavioral  
628 analyses carried out in P7 and P14 mice, where motor function in P7 Nav1.1<sup>cKO</sup> and Nav1.6<sup>cKO</sup>  
629 mice was largely intact but declined by P14 (Figs. S2 and S4). Interestingly, at P7 we observed  
630 little-to-no immunoreactivity of Nav1.1 or Nav1.6 in muscle spindles (Fig. S9). By P14, Nav1.6  
631 clusters begin to appear within the spindle, while Nav1.1 immunoreactivity remained weak. This  
632 suggests temporally distinct regulation of Nav localization at peripheral end organs compared to  
633 central circuits.

634

635 We find that loss of Nav1.6, but not Nav1.1, resulted in disrupted muscle spindle development. This  
636 is in line with recent findings that show mechanosensory neuron end organ development is activity  
637 dependent (21). Interestingly, previous work found deletion of Piezo2 in proprioceptors (Piezo2<sup>cKO</sup>)  
638 did not alter muscle spindle structure (5); however, these experiments were carried out in 4–5-  
639 week-old mice, whereas our analysis of muscle spindle structure was carried out in mice ages 8–12  
640 weeks. This raises the possibility that electrical activity is required for the maintenance, but not  
641 development, of muscle spindle structure.

642

643 Surprisingly, Nav1.6<sup>cKO</sup> mice showed significantly reduced skeletal muscle fiber size, highlighting  
644 a potential non-cell-autonomous role for proprioceptive feedback in skeletal muscle development  
645 or maintenance (Figs. 7 and 10). This effect was not seen in Nav1.1<sup>cKO</sup> mice, but is consistent with  
646 a study that found deletion of Piezo2 in proprioceptors led to non-cell-autonomous deficits in spine



647 alignment and hip joint formation (53). Despite the smaller size of Nav1.6<sup>CKO</sup> skeletal muscle fibers,  
648 all Nav1.6<sup>CKO</sup> intrinsic muscle properties were similar to Nav1.6<sup>het</sup> and Nav1.6<sup>fl/fl</sup> mice. Grip  
649 strength in Nav1.6<sup>CKO</sup> mice, however, was significantly weaker compared to other genotypes. These  
650 findings suggest that reduced grip strength in Nav1.6<sup>CKO</sup> mice is likely due to impaired motor neuron  
651 activation of skeletal muscle and not due to changes in intrinsic muscle function. Interestingly, prior  
652 studies have identified dysfunction in proprioceptive spinal cord circuits in mouse models of spinal  
653 muscular atrophy and amyotrophic lateral sclerosis (19, 54–56). An intriguing possibility is that  
654 loss of proprioceptive feedback onto motor neurons in Nav1.6<sup>CKO</sup> mice (Fig. 4) could lead to  
655 pathophysiological phenotypes similar to those observed in neuromuscular or motor neuron disease.

656  
657 Mutations in the genes that encode Nav1.1 and Nav1.6, *Scn1a* and *Scn8a*, respectively, are strongly  
658 associated with neurological diseases in which ataxia and motor developmental delays are  
659 prominent clinical manifestations (12, 26, 46). How proprioceptor dysfunction contributes to these  
660 disorders is unknown. The majority of Dravet syndrome patients have complete loss-of-function  
661 (LOF) of one copy of *Scn1a*; conversely, patient reported mutational variants in *Scn8a* are  
662 predominately gain-of-function (GOF). Our previous work found that proprioceptor afferents from  
663 Nav1.1<sup>het</sup> mice also had impaired encoding static muscle stretch (7), suggesting that motor  
664 dysfunction in patients missing one functional copy of *Scn1a* could be in part sensory in nature;  
665 however, it is unclear how *Scn8a* GOF mutations would affect proprioceptor function. Patients  
666 harboring either *Scn1a* LOF and *Scn8a* GOF mutations have similar motor deficits (11); thus, one  
667 possibility is that *Scn8a* GOF mutations lead to use-dependent block of action potential firing in  
668 proprioceptors, which could contribute to the similar motor phenotypes observed in these different  
669 patient populations (11). Interestingly, there are a few reported cases of LOF mutations in *Scn8a*  
670 that lead to general ataxia (57), and our data suggest that proprioceptor dysfunction could contribute  
671 to their motor deficits.

672

673 In addition to Nav1.1 and Nav1.6, proprioceptors also express Nav1.7 (7). Mice and humans that  
674 lack Nav1.7 are insensitive to pain but do not exhibit prominent deficits in motor function, which  
675 suggests a limited role of Nav1.7 in mammalian proprioception (9, 10). Alternatively, Nav1.1 and  
676 Nav1.6 may compensate for the developmental loss of Nav1.7, which occurs in constitutive genetic  
677 mouse models and human patients. It is possible that acute deletion of Nav1.7 in proprioceptors  
678 could reveal a previously overlooked contribution of the channel to proprioceptor function. Indeed,  
679 we found that Nav1.7 channels contribute to roughly one third of the somal whole-cell sodium  
680 current in genetically identified proprioceptors (7). Thus, a role for Nav1.7 in mammalian  
681 proprioception remains enigmatic.

682

683 A current limitation of the present study is the use of a sensory-neuron wide genetic targeting  
684 strategy, which makes interpretation of motor behavior and skeletal muscle impairments  
685 confounded by the loss of Nav1.1 or Nav1.6 in other sensory neuron populations, namely touch  
686 receptors. As mentioned above, deletion of Nav1.1 or Nav1.6 selectively in proprioceptors is not  
687 possible with currently available genetic tools, as the access point for Cre-driven deletion,  
688 parvalbumin, is also expressed in neurons of brain and spinal cord that are important for motor  
689 function. Despite this limitation, the direct role of Nav1.1 and Nav1.6 in proprioceptors was  
690 examined at the functional level in *ex vivo* muscle nerve recordings and spinal cord  
691 electrophysiology experiments, as well as in the structural analysis of VGLUT1 identified muscle  
692 spindles. To investigate the role of Nav channels with spatial precision, future experiments will  
693 require intersectional strategies for selective gene manipulations in proprioceptors.

694

695 Our data demonstrate that Nav1.1 and Nav1.6 play distinct and nonredundant roles in mammalian  
696 proprioception. This work is the first to define how Navs uniquely shape somatosensory

697 transmission and is also the first to show that Navs occupy distinct cellular compartments in sensory  
698 neuron end organs. We predict our results are broadly applicable to other sensory neuron  
699 populations, namely mechanoreceptors, which also co-express Nav1.1 and Nav1.6. Furthermore,  
700 these data have important translational implications for understanding the motor deficits associated  
701 with Nav1.1 and Nav1.6 channelopathies.

702

## 703 **Materials and Methods**

### 704 **Experimental design**

#### 705 **Animals**

706  $Pirt^{cre}$  and  $Scn8a^{fl/fl}$  mice were a gift from Drs. Xinzhong Dong (Johns Hopkins University, 58) and  
707 Miriam Meisler (University of Michigan, 59), respectively.  $Scn1a^{fl/fl}$  (stock #041829-UCD) were  
708 purchased from the UC Davis MMRRC. All mice used are a C57BL/6J background (non-congenic).  
709 Genotyping was outsourced to Transnetyx. Animals use was conducted according to guidelines  
710 from the National Institutes of Health's Guide for the Care and Use of Laboratory Animals and was  
711 approved by the Institutional Animal Care and Use Committee of UC Davis (#23049) and San Jose  
712 State University (#990, *ex vivo* muscle recordings.)  $Nav1.6^{cKO}$  mice were provided with wet food  
713 and hydrogels daily. Mice were maintained on a 12hr light/dark cycle, and food and water were  
714 provided ad libitum.

715

#### 716 **Animal behavior**

717 Motor function was tested using three assays: rotarod, open-field, and grip strength. Behavioral  
718 assays were conducted from least to most invasive in the order of open field, grip strength, and  
719 rotarod. All behavioral assays were conducted between 8-10 weeks of age and the experimenter  
720 was blind to genotype. For the open field, mice were acclimated to the behavior room for 1 h prior  
721 testing. The open field apparatus consisted of a white square box with dimensions of 15x15x20  
722 inches. A camera suspended above the open field tracked animal movement for a single 10-minute  
723 period using ANY-maze software. Following testing in the open field, mice were transported to a  
724 separate behavior room and allowed to acclimate for 1 h before being assayed in the grip strength  
725 and rotarod tests. A grip strength apparatus (IITC Life sciences, Woodland Hills, CA) with a metal  
726 grate was used. Mice held from the tail were placed on the metal grate and pulled horizontally away  
727 from apparatus once all four paws touched the grate. Mice were assayed across 6 trials with 5-

728 minute intervals between trials. A rotarod machine (IITC) that has an accelerating rotating cylinder  
729 was used. Nav1.6<sup>CKO</sup> mice were excluded from rotarod testing due to severe motor coordination  
730 deficits that prevented them from maintaining balance on the cylinder even in the absence of  
731 cylinder rotation. The averages of three trials across three consecutive training days were recorded.

### 732 ***Ex vivo* muscle nerve recordings**

733 Detailed methods on *ex vivo* muscle nerve recordings can be found in Wilkinson et al. 2012 (16).  
734 Briefly, extensor digitorum muscle and innervating peroneal branch of the sciatic nerve were  
735 dissected from adult mice and placed in a tissue bath of oxygenated Synthetic Interstitial Fluid at  
736 24°C. Tendons were tied to a fixed post and lever arm of a dual force and length controller and  
737 transducer (300C-LR, Aurora Scientific, Inc.). The cut end of the nerve was suctioned into a bipolar  
738 glass electrode and connected to an extracellular amplifier with headstage (Model 1800, A-M  
739 Systems). Muscles were held at the length of maximal twitch contraction, Lo. For static stretch  
740 experiments, nine 4 s ramp-and-hold stretches were given at 2.5, 5, and 7.5% of Lo (Ramp speed  
741 was 40% Lo/s). Stretch lengths were repeated three times. For sinusoidal stimuli, sixteen 9 s  
742 sinusoidal vibrations were given at 5, 25, 50, and 100  $\mu\text{m}$  amplitudes at varying frequencies (10,  
743 25, 50, and 100 Hz). A rest period of 1 min was given between each length change. Resting  
744 discharge was quantified as the firing rate 10 s before stretch. Firing rate during the static phase of  
745 stretch was calculated 3.25-3.75 sec into the hold phase of stretch (LabChart Software,  
746 ADInstruments). The consistency of firing during static muscle stretch was found by calculating  
747 the interspike interval coefficient of variation during the plateau phase of stretch ( $\text{CV} = \text{Std}$   
748  $\text{Dev}/\text{Mean}$  of ISI 1.5 – 3.5s after ramp up). For dynamic responses, the average firing rates during  
749 the 9 s vibration was determined. Entrainment was defined as whether a unit could entrain in a 1:1  
750 fashion to vibration stimulus. In most afferents we confirmed that they were Group Ia or II afferents  
751

752 by looking for a pause in firing during the shortening phase of contraction (a train of 60 stimulations  
753 of 0.5 ms pulse width were given at 1 Hz frequency from a 701C stimulator (Aurora Scientific)).

### 754 755 **Spinal cord electrophysiology**

756 Spinal cords were harvested from postnatal mice spanning the age-groups P6-11 and P14-18. The  
757 mice were deeply anesthetized with isoflurane, decapitated and eviscerated. We followed the  
758 protocol that has been used to record motor activity from mice of weight-bearing age using *ex vivo*  
759 spinal cord preparations (60, 61). In brief, after evisceration, the preparation was pinned to a  
760 dissecting chamber and continuously perfused with ice-cold solution, comprising (in mM): 188  
761 sucrose, 25 NaCl, 1.9 KCl, 10 MgSO<sub>4</sub>, 0.5 NaH<sub>2</sub>PO<sub>4</sub>, 26 NaHCO<sub>3</sub>, 1.2 NaH<sub>2</sub>PO<sub>4</sub>, 25 glucose,  
762 bubbled with 95 % O<sub>2</sub>/ 5 % CO<sub>2</sub>. The spinal cord was exposed following a ventral laminectomy  
763 and transected at the thoracic levels (T5-T8). The dorsal and ventral roots were isolated over the  
764 sixth lumbar segment, bilaterally, just proximal to the dorsal root ganglion. All other dorsal and  
765 ventral roots were trimmed, and the entire cord was removed from the vertebral column together  
766 with the attached roots and transferred to the recording chamber and continuously superfused with  
767 artificial cerebrospinal fluid (aCSF; concentrations in mM): 128 NaCl, 4 KCl, 1.5 CaCl<sub>2</sub>, 1 MgSO<sub>4</sub>,  
768 0.5 NaH<sub>2</sub>PO<sub>4</sub>, 21 NaHCO<sub>3</sub>, 30 D-glucose) bubbled with 95 % O<sub>2</sub> – 5 % CO<sub>2</sub>. A midsagittal  
769 hemisection was performed and the spinal hemicords were allowed to equilibrate in aCSF  
770 maintained at ambient temperature. After spinal cord isolation, dorsal and ventral roots at the sixth  
771 lumbar segment (L6) were placed into suction electrodes. The dorsal root was stimulated with  
772 single pulse stimulus, delivered every 30s, over 10 trials. The stimulus was delivered using a  
773 stimulus isolator unit (A365, World Precision Instruments) with current pulse amplitudes set at  
774 twice the threshold intensity of stimulation (2T, 0.1 ms pulse-width). Extracellular recordings were  
775 made at the ventral roots, the signal was filtered between 0.1–5000 Hz, amplified 1000 times  
776 (Model 1700, A-M Systems), digitized at 10 kHz using Digidata 1440A, acquired using Clampex

777 software (v11.2, Molecular Devices), and saved on a computer for offline analysis. Stretch reflex  
778 parameters were extracted from the signals for each experiment, after averaging over the 10 trials,  
779 using Clampfit (v11.2, Molecular Devices).

780

## 781 **Muscle Mechanics**

782 Soleus muscles were prepared for *ex vivo* passive mechanical testing as previously described (62).  
783 Briefly, 7-0 sutures were cinched at the muscle-tendon of the soleus and EDL muscles. Suture loops  
784 were placed on hooks connected to the 300C-LR-Dual-Mode motor arm and force transducer  
785 (Aurora Scientific) such that the muscle remained within 28°C oxygenated Ringer's solution.  
786 Twitches were induced using a 701C stimulator (Aurora Scientific) across a range of muscle lengths  
787 to determine the optimal length for isometric force generation ( $L_0$ ). The  $L_0$  length corresponded to  
788 the length between the sutures on either muscle-tendon junction, as measured by calipers.  
789 Physiological cross-sectional area (PCSA) was calculated using the muscle length ( $L_m$ ), mass ( $m$ ),  
790 ratio of fiber length to  $L_0$  ( $L_f/L_0$ ) and standard density of muscle ( $\rho=1.06 \text{ g/cm}^3$ ;  $\text{PCSA} =$   
791  $m/L_0*(L_f/L_0)*\rho$ , (63).

792

793 Soleus muscles were subjected to active mechanical testing, which consisted of a series of 24  
794 maximum isometric tetani (300 mA, 0.3 ms pulse width, 80 Hz pulse frequency, 800 ms pulse train)  
795 with 6 seconds of recovery in between each tetanus. Muscles were then given 300 seconds to  
796 recover before a final tetanus with the same parameters. Maximum isometric force was measured  
797 during the first, penultimate, and final tetanus protocol. Maximum forces were normalized to PCSA  
798 to give isometric specific tension. The highest isometric specific tension measured during each  
799 active protocol was reported as the isometric specific tension for each muscle. The percent of force  
800 maintained at the penultimate tetanus compared to the initial tetanus was recorded as the percent  
801 force post-fatigue. The percent of force maintained at the final tetanus compared to the initial

802 tetanus was recorded as the percent force post-recovery. After active mechanical testing was  
803 completed, muscles were removed from the mechanical testing equipment, embedded in OCT, and  
804 flash frozen in liquid nitrogen cooled isopentane. Muscles were stored at  $-70^{\circ}\text{C}$  until  
805 cryosectioning.

806

### 807 **Tissue Processing.**

808 For muscle spindle immunolabeling experiments, mice were anesthetized using a  
809 ketamine/xylazine cocktail and transcardially perfused with PBS followed by 1% PFA. Extensor  
810 digitorum longus (EDL) muscle was then dissected in PBS and post-fixed for 30 min then washed  
811 in PBS before incubation in 30% sucrose solution overnight at 4C. Following cryoprotection,  
812 muscles were embedded in optimal cutting temperature (Fisher #4585) and stored in  $-80\text{C}$  until  
813 sectioning.

814

### 815 **Immunohistochemistry.**

816 For immunolabeling experiments in muscle spindles, EDL muscles were sectioned ( $30\mu\text{m}$ ) along  
817 the longitudinal axis. Tissue was incubated in blocking solution (0.1% PBS-T/5% normal goat  
818 serum in PBS) and the following primary antibodies were used: guinea pig anti-VGLUT1 (1:8000,  
819 Zuckerman Institute 1705) and rabbit anti- $\beta$ III tubulin (1:3000, Abcam #ab18207). Secondaries are  
820 as follows: anti-guinea pig 488 (1:1000, Thermo Fisher, A11073) and anti-rabbit 647 (1:1000,  
821 A32733). For muscle fiber typing experiments, soleus cross sections ( $20\mu\text{m}$ ) were blocked in a  
822 solution containing 5% BSA in PBS. The following primary antibodies were diluted and incubated  
823 on muscle sections overnight: mouse IgG2b anti-myosin heavy chain type I (1:250, BA-F8, DHSB)  
824 and mouse IgG1 anti-myosin heavy chain type IIa (1:250, SC-71, DHSB). Slides were washed in  
825 PBS and the following secondaries were diluted in 2% BSA and incubated for 60 minutes: goat  
826 anti-mouse IgG2b 488 (1:500, A21141) goat anti-mouse IgG1 555 (1:500 A21127). After



827 secondary antibody incubation slides were washed in PBS and mounted with FluoromountG with  
828 DAPI (SouthernBiotech 0100-20). For immunolabeling of Navs the following primary antibodies  
829 were used: guinea pig anti-VGLUT1 (1:8000, Zuckerman Institute 1705), rabbit anti-Nav1.1  
830 (2ug/ml, Neuromab A11954), mouse IgG1 anti-Nav1.6, mouse (6ug/ml, Neuromab K87A/10.2),  
831 rabbit anti-Nav1.6 (1:750, Alomone, ASC009), IgG2a anti-Ankyrin G (6ug/ml, N106/36.1), and  
832 chicken anti-neurofilament heavy (1:3000, Abcam ab4680). Secondaries used were as follows: anti-  
833 guinea pig 488 (1:1000, Thermo Fisher, A11073), mouse anti-IgG1 555 (1:1000, A21137), mouse  
834 anti IgG2a-647 (1:1000, A21240), anti-chicken 594 (1:1000, WA316328). All specimens were  
835 imaged in three dimensions on either a Zeiss LSM880 Airyscan (63x oil objective, 1.4 NA) or  
836 Olympus LV3000 (60x oil objective, 1.4 NA) confocal microscope. Images were analyzed using  
837 ImageJ software.

### 838

### 839 **Analysis of muscle spindle structure.**

840 Disruptions in muscle spindle sensory endings were quantified by colocalizing VGLUT1  
841 immunoreactivity with DAPI to calculate a wrapping efficiency index (WEI). Intrafusal muscle  
842 fibers are identifiable in skeletal muscle based on mono- and bi-nucleation via DAPI<sup>+</sup> staining. To  
843 analyze muscle spindle sensory wrappings without bias, we only analyzed sensory wrappings  
844 VGLUT1 sensory wrappings that overlapped with DAPI labeling. For example, in ImageJ, regions  
845 of interest (ROIs) were drawn around each sensory wrapping. If the ROI did not overlap with DAPI,  
846 it was not counted as a sensory wrapping and was excluded from the analysis. The total number of  
847 sensory wrappings (n) were counted and normalized to muscle spindle length (l). The following  
848 equation was used to calculate the WEI:

$$849 \quad WEI = n/l$$

### 850

### 851 **Experimental Design and statistical analysis.**

852 Summary data are presented as mean  $\pm$  SD, from n cells, afferents, sections, or N animals. All  
853 analysis of immunofluorescent images contained at least 3 biological replicates per condition.  
854 Investigator was blinded to genotypes during analysis. For all behavioral, electrophysiological, and  
855 mechanics experiments the investigator was blind to genotype. To determine differences in  
856 entrainment properties between Nav1.6<sup>fl/fl</sup>, Nav1.6<sup>het</sup>, and Nav1.6<sup>cKO</sup> we used a logistic regression  
857 analysis (SPSS), is a statistical model that calculates the log-odds of an event (i.e. entrainment or  
858 non-entrainment) as a linear combination of one or more independent variables (vibration  
859 frequency, vibration amplitude and genotype). All other statistical testing was carried out using  
860 Prism 10.1 (Graphpad software). Statistical differences were determined using parametric tests for  
861 normally distributed data and nonparametric tests for data that did not conform to Gaussian  
862 distributions or had different variances. Statistical significance in each case is denoted as follows:  
863 \*p<0.05, \*\*p<0.01, \*\*\*p<0.001, and \*\*\*\*p<0.0001. Source files for each figure can be found on  
864 Mendeley.

865

## 866 References

- 867 1. U. Proske, S. C. Gandevia, The proprioceptive senses: their roles in signaling body shape,  
868 body position and movement, and muscle force. *Physiol. Rev.* **92**, 1651–1697 (2012).
- 869 2. J. C. Tuthill, E. Azim, Proprioception. *Curr. Biol.* **28**, R194–R203 (2018).
- 870 3. K. A. Wilkinson, Molecular determinants of mechanosensation in the muscle spindle. *Curr.*  
871 *Opin. Neurobiol.* **74**, 102542 (2022).
- 872 4. D. Florez-Paz, K. K. Bali, R. Kuner, A. Gomis, A critical role for Piezo2 channels in the  
873 mechanotransduction of mouse proprioceptive neurons. *Sci. Rep.* **6**, 25923 (2016).
- 874 5. S.-H. Woo, V. Lukacs, J. C. de Nooij, D. Zaytseva, C. R. Criddle, A. Francisco, T. M.  
875 Jessell, K. A. Wilkinson, A. Patapoutian, Piezo2 is the principal mechanotransduction  
876 channel for proprioception. *Nat. Neurosci.* **18**, 1756–1762 (2015).
- 877 6. A. T. Chesler, M. Szczot, D. Bharucha-Goebel, M. Čeko, S. Donkervoort, C. Laubacher, L.  
878 H. Hayes, K. Alter, C. Zampieri, C. Stanley, A. M. Innes, J. K. Mah, C. M. Grosmann, N.  
879 Bradley, D. Nguyen, A. R. Foley, C. E. Le Pichon, C. G. Bönnemann, The Role of PIEZO2  
880 in Human Mechanosensation. *N. Engl. J. Med.* **375**, 1355–1364 (2016).
- 881 7. C. M. Espino, C. M. Lewis, S. Ortiz, M. S. Dalal, S. Garlapalli, K. M. Wells, D. A. O’Neil,  
882 K. A. Wilkinson, T. N. Griffith, Nav1.1 is essential for proprioceptive signaling and motor  
883 behaviors. *Elife* **11** (2022).
- 884 8. S. D. Dib-Hajj, A. M. Rush, T. R. Cummins, F. M. Hisama, S. Novella, L. Tyrrell, L.  
885 Marshall, S. G. Waxman, Gain-of-function mutation in Nav1.7 in familial erythromelalgia  
886 induces bursting of sensory neurons. *Brain* **128**, 1847–1854 (2005).
- 887 9. J. J. Cox, F. Reimann, A. K. Nicholas, G. Thornton, E. Roberts, K. Springell, G. Karbani, H.  
888 Jafri, J. Mannan, Y. Raashid, L. Al-Gazali, H. Hamamy, E. M. Valente, S. Gorman, R.  
889 Williams, D. P. McHale, J. N. Wood, F. M. Gribble, C. G. Woods, An SCN9A  
890 channelopathy causes congenital inability to experience pain. *Nature* **444**, 894–898 (2006).
- 891 10. J. Gingras, S. Smith, D. J. Matson, D. Johnson, K. Nye, L. Couture, E. Feric, R. Yin, B. D.  
892 Moyer, M. L. Peterson, J. B. Rottman, R. J. Beiler, A. B. Malmberg, S. I. McDonough,  
893 Global Nav1.7 knockout mice recapitulate the phenotype of human congenital indifference  
894 to pain. *PLoS One* **9**, e105895 (2014).
- 895 11. M. H. Meisler, S. F. Hill, W. Yu, Sodium channelopathies in neurodevelopmental disorders.  
896 *Nat. Rev. Neurosci.* **22**, 152–166 (2021).
- 897 12. M. H. Meisler, J. Kearney, A. Escayg, B. T. MacDonald, L. K. Sprunger, Sodium channels  
898 and neurological disease: insights from Scn8a mutations in the mouse. *Neuroscientist* **7**,  
899 136–145 (2001).
- 900 13. S. I. Levin, Z. M. Khaliq, T. K. Aman, T. M. Grieco, J. A. Kearney, I. M. Raman, M. H.  
901 Meisler, Impaired motor function in mice with cell-specific knockout of sodium channel  
902 Scn8a (Nav1.6) in cerebellar purkinje neurons and granule cells. *J. Neurophysiol.* **96**, 785–  
903 793 (2006).

- 904 14. I. Ogiwara, H. Miyamoto, N. Morita, N. Atapour, E. Mazaki, I. Inoue, T. Takeuchi, S.  
905 Itohara, Y. Yanagawa, K. Obata, T. Furuichi, T. K. Hensch, K. Yamakawa, Nav1.1 localizes  
906 to axons of parvalbumin-positive inhibitory interneurons: a circuit basis for epileptic seizures  
907 in mice carrying an Scn1a gene mutation. *J. Neurosci.* **27**, 5903–5914 (2007).
- 908 15. B. Ferguson, C. Glick, J. R. Huguenard, Prefrontal PV interneurons facilitate attention and  
909 are linked to attentional dysfunction in a mouse model of absence epilepsy. *Elife* **12** (2023).
- 910 16. K. A. Wilkinson, H. E. Kloefkorn, S. Hochman, Characterization of muscle spindle afferents  
911 in the adult mouse using an in vitro muscle-nerve preparation. *PLoS One* **7**, e39140 (2012).
- 912 17. J. C. Eccles, R. M. Eccles, A. Lundberg, The convergence of monosynaptic excitatory  
913 afferents on to many different species of alpha motoneurons. *J. Physiol.* **137**, 22–50 (1957).
- 914 18. S. C. Mears, E. Frank, Formation of specific monosynaptic connections between muscle  
915 spindle afferents and motoneurons in the mouse. *J. Neurosci.* **17**, 3128–3135 (1997).
- 916 19. G. Z. Mentis, D. Blivis, W. Liu, E. Drobac, M. E. Crowder, L. Kong, F. J. Alvarez, C. J.  
917 Sumner, M. J. O’Donovan, Early functional impairment of sensory-motor connectivity in a  
918 mouse model of spinal muscular atrophy. *Neuron* **69**, 453–467 (2011).
- 919 20. K. M. Oliver, D. M. Florez-Paz, T. C. Badea, G. Z. Mentis, V. Menon, J. C. de Nooij,  
920 Molecular correlates of muscle spindle and Golgi tendon organ afferents. *Nat. Commun.* **12**,  
921 1451 (2021).
- 922 21. C. Santiago, N. Sharma, N. Africawala, J. Siegrist, A. Handler, A. Tasnim, R. Anjum, J.  
923 Turecek, B. P. Lehnert, S. Renauld, M. Nolan-Tamariz, M. Iskols, A. R. Magee, S. Paradis,  
924 D. D. Ginty, Activity-dependent development of the body’s touch receptors, *bioRxiv*  
925 (2023)p. 2023.09.23.559109.
- 926 22. L. W. Duchon, E. Stefani, Electrophysiological studies of neuromuscular transmission in  
927 hereditary “motor end-plate disease” of the mouse. *J. Physiol.* **212**, 535–548 (1971).
- 928 23. L. R. Smith, E. R. Barton, SMASH - semi-automatic muscle analysis using segmentation of  
929 histology: a MATLAB application. *Skelet. Muscle* **4**, 21 (2014).
- 930 24. I. Kwon, K. S. Kim, Y. Lee, Relationships between endurance exercise training-induced  
931 muscle fiber-type shifting and autophagy in slow- and fast-twitch skeletal muscles of mice.  
932 *Phys. Act. Nutr.* **28**, 23–34 (2024).
- 933 25. N. Haida, W. M. Fowler Jr, R. T. Abresch, D. B. Larson, R. B. Sharman, R. G. Taylor, R. K.  
934 Entrikin, Effect of hind-limb suspension on young and adult skeletal muscle. I. Normal mice.  
935 *Exp. Neurol.* **103**, 68–76 (1989).
- 936 26. F. Kalume, F. H. Yu, R. E. Westenbroek, T. Scheuer, W. A. Catterall, Reduced sodium  
937 current in Purkinje neurons from Nav1.1 mutant mice: implications for ataxia in severe  
938 myoclonic epilepsy in infancy. *J. Neurosci.* **27**, 11065–11074 (2007).
- 939 27. R. R. Patel, C. Barbosa, Y. Xiao, T. R. Cummins, Human Nav1.6 Channels Generate Larger  
940 Resurgent Currents than Human Nav1.1 Channels, but the Navβ4 Peptide Does Not Protect  
941 Either Isoform from Use-Dependent Reduction. *PLoS One* **10**, e0133485 (2015).

- 942 28. Z. M. Khaliq, N. W. Gouwens, I. M. Raman, The contribution of resurgent sodium current to  
943 high-frequency firing in Purkinje neurons: an experimental and modeling study. *J. Neurosci.*  
944 **23**, 4899–4912 (2003).
- 945 29. W. Hu, C. Tian, T. Li, M. Yang, H. Hou, Y. Shu, Distinct contributions of Na(v)1.6 and  
946 Na(v)1.2 in action potential initiation and backpropagation. *Nat. Neurosci.* **12**, 996–1002  
947 (2009).
- 948 30. A. Duflocq, B. Le Bras, E. Bullier, F. Couraud, M. Davenne, Nav1.1 is predominantly  
949 expressed in nodes of Ranvier and axon initial segments. *Mol. Cell. Neurosci.* **39**, 180–192  
950 (2008).
- 951 31. J. H. Caldwell, K. L. Schaller, R. S. Lasher, E. Peles, S. R. Levinson, Sodium channel  
952 Nav1.6 is localized at nodes of Ranvier, dendrites, and synapses. *Proceedings of the National*  
953 *Academy of Sciences* **97**, 5616–5620 (2000).
- 954 32. E. J. Akin, L. Solé, S. D. Dib-Hajj, S. G. Waxman, M. M. Tamkun, Preferential targeting of  
955 Nav1.6 voltage-gated Na<sup>+</sup> Channels to the axon initial segment during development. *PLoS*  
956 *One* **10**, e0124397 (2015).
- 957 33. A. N. King, C. F. Manning, J. S. Trimmer, A unique ion channel clustering domain on the  
958 axon initial segment of mammalian neurons: Ion channel clustering on the axon initial  
959 segment. *J. Comp. Neurol.* **522**, 2594–2608 (2014).
- 960 34. G. S. Bewick, R. W. Banks, Mechanotransduction in the muscle spindle. *Pflugers Arch.* **467**,  
961 175–190 (2015).
- 962 35. Y. Zheng, P. Liu, L. Bai, J. S. Trimmer, B. P. Bean, D. D. Ginty, Deep Sequencing of  
963 Somatosensory Neurons Reveals Molecular Determinants of Intrinsic Physiological  
964 Properties. *Neuron* **103**, 598-616.e7 (2019).
- 965 36. S. C. Koch, M. G. Del Barrio, A. Dalet, G. Gatto, T. Günther, J. Zhang, B. Seidler, D. Saur,  
966 R. Schüle, M. Goulding, ROR $\beta$  Spinal Interneurons Gate Sensory Transmission during  
967 Locomotion to Secure a Fluid Walking Gait. *Neuron* **96**, 1419-1431.e5 (2017).
- 968 37. M. A. Gradwell, N. Ozeri-Engelhard, J. T. Eisdorfer, O. D. Laflamme, M. Gonzalez, A.  
969 Upadhyay, L. Medlock, T. Shrier, K. R. Patel, A. Aoki, M. Gandhi, G. Abbas-Zadeh, O.  
970 Oputa, J. K. Thackray, M. Ricci, A. George, N. Yusuf, J. Keating, Z. Imtiaz, S. A. Alomary,  
971 M. Bohic, M. Haas, Y. Hernandez, S. A. Prescott, T. Akay, V. E. Abaira, Multimodal  
972 sensory control of motor performance by glycinergic interneurons of the mouse spinal cord  
973 deep dorsal horn. *Neuron* **112**, 1302-1327.e13 (2024).
- 974 38. S. Kröger, B. Watkins, Muscle spindle function in healthy and diseased muscle. *Skelet.*  
975 *Muscle* **11**, 3 (2021).
- 976 39. J. Desaki, N. Nishida, A further observation of muscle spindles in the extensor digitorum  
977 longus muscle of the aged rat. *J. Electron Microsc. (Tokyo)* **59**, 79–86 (2010).
- 978 40. L. Gerwin, S. Rossmann, C. Haupt, J. Schultheiß, H. Brinkmeier, R. E. Bittner, S. Kröger,  
979 Impaired muscle spindle function in murine models of muscular dystrophy. *J. Physiol.* **598**,  
980 1591–1609 (2020).

- 981 41. T. N. Griffith, T. A. Docter, E. A. Lumpkin, Tetrodotoxin-Sensitive Sodium Channels  
982 Mediate Action Potential Firing and Excitability in Menthol-Sensitive Vglut3-Lineage  
983 Sensory Neurons. *J. Neurosci.* **39**, 7086–7101 (2019).
- 984 42. B. Drouillas, C. Brocard, S. Zanella, R. Bos, F. Brocard, Persistent Nav1.1 and Nav1.6  
985 currents drive spinal locomotor functions through nonlinear dynamics. *Cell Rep.* **42**, 113085  
986 (2023).
- 987 43. J. E. O'Brien, M. H. Meisler, Sodium channel SCN8A (Nav1.6): properties and de novo  
988 mutations in epileptic encephalopathy and intellectual disability. *Front. Genet.* **4**, 213  
989 (2013).
- 990 44. T. Boiko, A. Van Wart, J. H. Caldwell, S. R. Levinson, J. S. Trimmer, G. Matthews,  
991 Functional specialization of the axon initial segment by isoform-specific sodium channel  
992 targeting. *J. Neurosci.* **23**, 2306–2313 (2003).
- 993 45. D. P. Schafer, A. W. Custer, P. Shrager, M. N. Rasband, Early events in node of Ranvier  
994 formation during myelination and remyelination in the PNS. *Neuron Glia Biol.* **2**, 69–79  
995 (2006).
- 996 46. F. H. Yu, M. Mantegazza, R. E. Westenbroek, C. A. Robbins, F. Kalume, K. A. Burton, W.  
997 J. Spain, G. S. McKnight, T. Scheuer, W. A. Catterall, Reduced sodium current in  
998 GABAergic interneurons in a mouse model of severe myoclonic epilepsy in infancy. *Nat.*  
999 *Neurosci.* **9**, 1142–1149 (2006).
- 1000 47. S. R. Stevens, M. N. Rasband, Ankyrins and neurological disease. *Curr. Opin. Neurobiol.*  
1001 **69**, 51–57 (2021).
- 1002 48. C. Zhang, A. Joshi, Y. Liu, O. Sert, S. G. Haddix, L. H. Teliska, A. Rasband, G. G. Rodney,  
1003 M. N. Rasband, Ankyrin-dependent Na<sup>+</sup> channel clustering prevents neuromuscular synapse  
1004 fatigue. *Curr. Biol.* **31**, 3810–3819.e4 (2021).
- 1005 49. A. Van Wart, T. Boiko, J. S. Trimmer, G. Matthews, Novel clustering of sodium channel  
1006 Na(v)1.1 with ankyrin-G and neurofascin at discrete sites in the inner plexiform layer of the  
1007 retina. *Mol. Cell. Neurosci.* **28**, 661–673 (2005).
- 1008 50. F. Laezza, B. R. Gerber, J.-Y. Lou, M. A. Kozel, H. Hartman, A. M. Craig, D. M. Ornitz, J.  
1009 M. Nerbonne, The FGF14(F145S) mutation disrupts the interaction of FGF14 with voltage-  
1010 gated Na<sup>+</sup> channels and impairs neuronal excitability. *J. Neurosci.* **27**, 12033–12044 (2007).
- 1011 51. L. L. Isom, Sodium channel beta subunits: anything but auxiliary. *Neuroscientist* **7**, 42–54  
1012 (2001).
- 1013 52. S. Luo, M. Jaegle, R. Li, G. R. Ehring, D. Meijer, S. R. Levinson, The sodium channel  
1014 isoform transition at developing nodes of Ranvier in the peripheral nervous system:  
1015 dependence on a Genetic program and myelination-induced cluster formation. *J. Comp.*  
1016 *Neurol.* **522**, 4057–4073 (2014).
- 1017 53. E. Assaraf, R. Blecher, L. Heinemann-Yerushalmi, S. Krief, R. Carmel Vinestock, I. E.  
1018 Biton, V. Brumfeld, R. Rotkopf, E. Avisar, G. Agar, E. Zelzer, Piezo2 expressed in  
1019 proprioceptive neurons is essential for skeletal integrity. *Nat. Commun.* **11**, 3168 (2020).

- 1020 54. M. A. Rubio, M. Herrando-Grabulosa, X. Navarro, Sensory involvement in amyotrophic  
1021 lateral sclerosis. *Int. J. Mol. Sci.* **23**, 15521 (2022).
- 1022 55. R. Aishwarya, C. S. Abdullah, N. S. Remex, S. Nitu, B. Hartman, J. King, M. A. N.  
1023 Bhuiyan, O. Rom, S. Miriyala, M. Panchatcharam, A. W. Orr, C. G. Kevil, M. S. Bhuiyan,  
1024 Pathological sequelae associated with skeletal muscle atrophy and histopathology in  
1025 G93A\*SOD1 mice. *Muscles* **2**, 51–74 (2023).
- 1026 56. E. V. Fletcher, C. M. Simon, J. G. Pagiazitis, J. I. Chalif, A. Vukojicic, E. Drobac, X. Wang,  
1027 G. Z. Mentis, Reduced sensory synaptic excitation impairs motor neuron function via Kv2.1  
1028 in spinal muscular atrophy. *Nat. Neurosci.* **20**, 905–916 (2017).
- 1029 57. J. L. Wagnon, N. E. Mencacci, B. S. Barker, E. R. Wengert, K. P. Bhatia, B. Balint, M.  
1030 Carecchio, N. W. Wood, M. K. Patel, M. H. Meisler, Partial loss-of-function of sodium  
1031 channel SCN8A in familial isolated myoclonus. *Hum. Mutat.* **39**, 965–969 (2018).
- 1032 58. A. Y. Kim, Z. Tang, Q. Liu, K. N. Patel, D. Maag, Y. Geng, X. Dong, Pirt, a  
1033 phosphoinositide-binding protein, functions as a regulatory subunit of TRPV1. *Cell* **133**,  
1034 475–485 (2008).
- 1035 59. S. I. Levin, M. H. Meisler, Floxed allele for conditional inactivation of the voltage-gated  
1036 sodium channel Scn8a (Nav1.6). *Genesis* **39**, 234–239 (2004).
- 1037 60. Z. Jiang, K. P. Carlin, R. M. Brownstone, An in vitro functionally mature mouse spinal cord  
1038 preparation for the study of spinal motor networks. *Brain Res.* **816**, 493–499 (1999).
- 1039 61. C. Nagaraja, Ventral root evoked entrainment of disinhibited bursts across early postnatal  
1040 development in mice. *IBRO Rep* **9**, 310–318 (2020).
- 1041 62. R. P. Wohlgemuth, R. M. Feitzinger, K. E. Henricson, D. T. Dinh, S. E. Brashear, L. R.  
1042 Smith, The extracellular matrix of dystrophic mouse diaphragm accounts for the majority of  
1043 its passive stiffness and is resistant to collagenase digestion. *Matrix Biol Plus* **18**, 100131  
1044 (2023).
- 1045 63. J. Mendez, A. Key, *Density and Composition of Mammalian Muscle*. *Metabolism*. 9(2):184-  
1046 188. (1960).

1047 **Acknowledgments**

1048 We would like to thank Drs. Xinzhong Dong and Miram Meisler for sharing mouse lines,  
1049 and Dr. James Trimmer for providing support and guidance on immunolabeling  
1050 experiments. Thanks to Griffith and Contreras Lab members for helpful discussions.  
1051 Additional support was provided by. Core facilities were supported by P30 EY12576.  
1052

1053 **Funding:** This study was supported by the National Institute General Medical Sciences  
1054 (T32GM099608, T32GM1144303, CME; R16GM153600, KAW; R25GM116690, ELM),  
1055 National Institute of Neurological Disease and Stroke (F31NS134241, CME;  
1056 R25NS112130, YM; R01NS135005, TNG; K01NS124828, TNG), and the National  
1057 Institute of Arthritis and Musculoskeletal and Skin Diseases (R01AR079545, LRS,  
1058 F31AR082695, RPW), and the Department of Defense (MD210110, LRS). Additional  
1059 support was provided by The Doris Duke Charitable Foundation COVID-19 Fund to Retain  
1060 Clinical Scientists awarded to UC Davis School of Medicine by the Burroughs Wellcome  
1061 Fund (TNG).  
1062

1063 **Author contributions:**

1064 Conceptualization: CME, TNG

1065 Methodology: CME, CN, SO, JRD, ARM, YM, ELM, SG, RPW, SEB, LS, KW,  
1066 TNG

1067 Investigation: CME, CN, SO, JRD, ARM, YM, ELM, SG, RPW, SEB

1068 Visualization: CME, TNG

1069 Supervision: CME, TNG

1070 Writing—original draft: CME

1071 Writing—review & editing: CME, TNG  
1072

1073 **Competing interests:** All other authors declare they have no competing interests  
1074

1075 **Data and materials availability:** All data are available in the main text or the  
1076 supplementary materials. Source data for each figure can be found on Mendeley.  
1077



1078  
1079  
1080  
1081  
1082  
1083  
1084  
1085  
1086  
1087  
1088  
1089  
1090  
1091  
1092  
1093  
1094  
1095  
1096  
1097  
1098  
1099  
1100  
1101  
1102  
1103  
1104  
1105  
1106

## Supplementary Materials for

### **Differential encoding of mammalian proprioception by voltage-gated sodium channels.**

Espino et al.

\*Corresponding author: Theanne Griffith

Email: [tgriffith@ucdavis.edu](mailto:tgriffith@ucdavis.edu)

#### **This PDF file includes:**

- Supplementary Methods
- Figs. S1 to S11
- Table S1
- Movies S1 to S2

#### **Other Supplementary Materials for this manuscript include the following:**

- Movies S1 to S2

## 1107 **Supplementary Materials**

## 1108 **Supplementary Methods**

### 1109 **Assessment of motor function during at postnatal day 7 and 14.**

1110 Floxed, heterozygous, and conditional knockout P7 and P14 pups from the Nav1.1 and Nav1.6 mouse lines were  
1111 assayed for motor dysfunction. The experimenter was blind to genotype.

### 1112 **Behavioral assays at postnatal day 7:**

1113  
1114 Hindlimb foot angle: In a clear empty mouse cage, a camera was positioned from below and above to record the pup  
1115 as it moved around the cage. The pup was gently prodded by touching its tail to motivate the pup to move. An average  
1116 of three pictures were taken from above and below. Using the acquired pictures, measures of the foot angle of the pups  
1117 were performed using Fiji ImageJ software by drawing a line from the end of the heel/shin to the tip of the middle toe  
1118 on each hindlimb and measuring the angle of the intersecting lines. Measurements were only taken when the pup was  
1119 performing a full stride in a straight line and both feet were flat on the ground. Three to five sets of foot angles were  
1120 measured per pup and used to calculate the average angle for each pup tested.

1121  
1122 Righting reflex: Pups were placed on their backs on a bench pad and held in that position for 5 seconds. The pups were  
1123 released, and the time it took for the pup to return to the prone position was recorded. This was repeated for a total of  
1124 three trials and the average righting reflex latency was calculated. Intertrial rest periods were 60 seconds.

1125  
1126 Hindlimb strength: Using a 50ml conical tube with cotton ball padding at the bottom, the pup was gently placed face  
1127 down into the tube with its hind limbs hung over the rim. The latency for the pup to fall into the tube was recorded.  
1128 The test was ended at 60 seconds if the pup did not fall. Each pup was only tested one time to avoid exhaustion.

1129  
1130 Grasping reflex: Pups were held by the scruff of the neck in a similar way to the how it is carried by the mother. The  
1131 pad of each individual mouse paw was stroked using the wooden stick of a cotton tip applicator. The grasp reflex was  
1132 determined present if the mouse paw curled around the wooden stick. Mice received a score of zero if all four paws  
1133 had the grasp reflex present, a score of 1 if one paw did not have the grasp reflex present, a score of 2 if two paws did  
1134 not have the grasp reflex present, and score of 3 if three paws did not have the grasp reflex present, and a score of 4 if  
1135 four paws did not have the grasp reflex present.

### 1136 **Behavioral assay at postnatal day 14**

1137  
1138 Modified limb coordination assay: This test was used to determine differences in grip, balance and limb coordination  
1139 at postnatal day 14. Pups were placed on a wire grid with metal poles running parallel to each other, approximately 8  
1140 millimeters apart with a diameter of 3 millimeters. The pups were left on the grid for five seconds and were scored by  
1141 their ability to grip and balance with each individual limb without the paw slipping in between the metal bars. Pups  
1142 that could grip/balance with all four limbs received a score of 0, pups that could grip/balance with only three limbs  
1143 received a score of 1, pups that could grip/balance with only two limbs received a score of 2, Pups that could  
1144 grip/balance with only one limb received a score of 3, and pups that could grip/balance with none of their limbs received  
1145 a score of 4. The assay was repeated a total of three times with 30 seconds in between tests, and the average of the three  
1146 trials was reported.

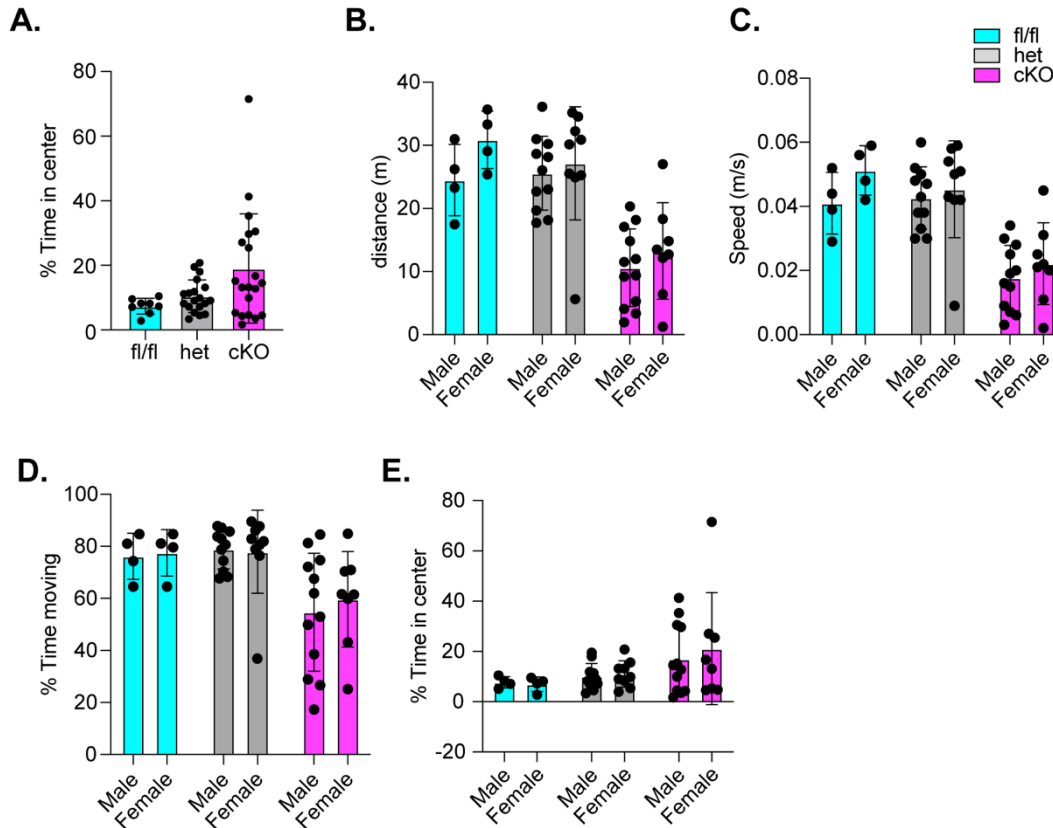
1147  
1148 **Multiplex *in situ* hybridization.** DRG were harvested from adult (10-15 week-old) Pirt<sup>Cre</sup>;Nav1.6<sup>fl/fl</sup> mice of both  
1149 sexes. DRG was sectioned at 25  $\mu$ m sections and were processed for RNA *in situ* detection using a modified version  
1150 of manufacture protocol (Advanced Cell Diagnostics) as previously described (Griffith 2019 and Espino 2022). The  
1151 following probes were used: Pvalb (421931C1, mouse) and Runx3 (451271-C3, mouse). Following *in situ*  
1152 hybridization, sections were incubated in blocking solution (5% NGS, 0.1% PBS-T) for 1hr at room temperature (RT).  
1153 Tissue was incubated in rabbit  $\beta$ III-Tubulin primary antibodies (1:3000, Abcam ab41489) overnight at 4°C overnight.  
1154 Tissue was treated with anti-rabbit 594 (1:1000, Invitrogen, A11037) secondary antibodies for 30 min at RT. Sections  
1155 were mounted with Fluoromount-G with DAPI and imaged in three dimensions on Olympus confocal (FV3000) using  
1156 40x 0.90 NA water objective lens. Images were analyzed using ImageJ software.

1157  
1158 **Immunolabeling of muscle spindles in postnatal development.** Immunohistochemistry of EDL harvested from P7  
1159 and P14 C57Bl6/J mice was performed. EDL was sectioned (25  $\mu$ m) on a cryostat and sections were labeled using the  
1160 following primary antibodies: rabbit polyclonal Nav1.1 (2 $\mu$ L/mL, Neuromab, NACH AP11954), guinea pig anti-  
1161 VGLUT1 (1:8000, Zuckerman Institute, 1705), and chicken anti-NFH (1:3000, Abcam, ab4680), rabbit polyclonal anti-  
1162 Nav1.6 (1:750, Alomone Labs, ASC-009). Secondary antibodies used were as follows: anti-rabbit 594 (1:500, Thermo  
1163 Fisher, A32740), anti-guinea pig 647 (1:1000, Thermo Fisher, A11073), and anti-chicken 647 (Thermo Fisher,  
1164

1165 A32733), anti-mouse IgG2a 555 (A21137). Specimens were mounted with Fluoromount-G with DAPI  
1166 (SouthernBiotech, 0100-20). All specimens were imaged in three dimensions on an Olympus FV3000 confocal  
1167 microscope using 60x NA 1.4 oil objective lens. Images were analyzed using ImageJ software.

1168

1169 **Supplementary figure and legends**



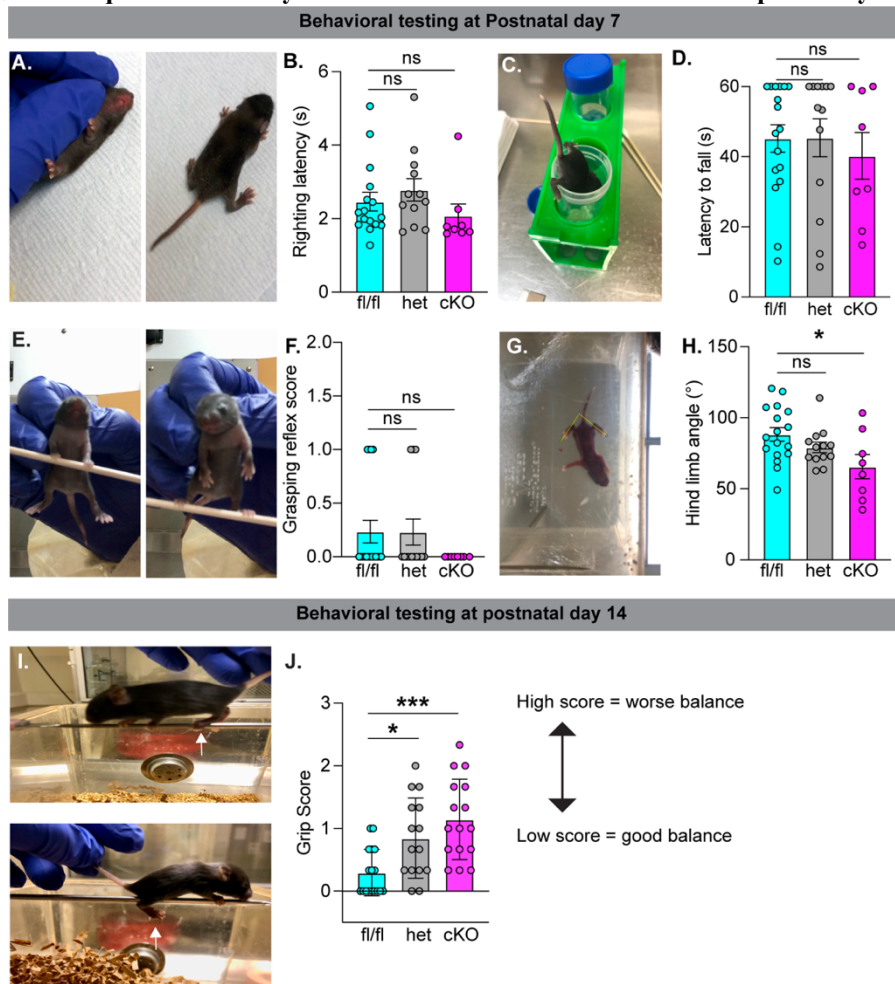
1170

1171 **Fig. S1. Motor behavior analysis of mice lacking Nav1.6 in sensory neurons**

1172 (A) Quantification of percent time spent in the center during a 10 min open-field trial. A Kruskal-  
1173 Wallis test with Dunn's Post-hoc comparison was used to determine statistical significance.  
1174 Nav1.6<sup>het</sup> p=0.4206, Nav1.6<sup>cKO</sup> p=0.1026 compared to Nav1.6<sup>fl/fl</sup>. Nav1.6<sup>fl/fl</sup> n = 8, Nav1.6<sup>het</sup> n=20,  
1175 Nav1.6<sup>cKO</sup> n =20. No significant differences were observed for motor behaviors male and female  
1176 mice of all genotypes. (B) Distance moved. (C) Speed. (D) Percent time moving. (E) Percent time  
1177 spend in center.  
1178

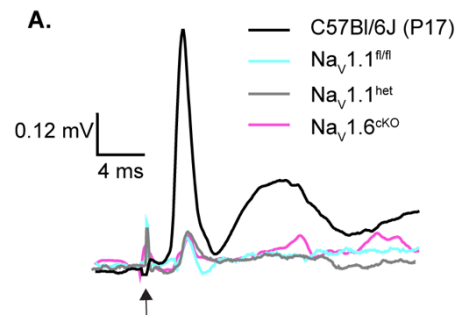
1179

**Fig. S2. Nav1.6 is required in sensory neurons for motor behaviors in a developmentally dependent manner.**



1180 (A to H) Behavioral testing on mice age P7, N=17 Nav1.6<sup>fl/fl</sup>, N= 13 Nav1.6<sup>het</sup>, and N= 8 Nav1.6<sup>cKO</sup>.  
 1181 (A) Representative images of righting reflex before (left) and after (right). (B) Latency for mice to  
 1182 right themselves was quantified. Nav1.6<sup>het</sup> (grey, p=0.686), Nav1.6<sup>cKO</sup> (magenta, p=0.655)  
 1183 compared to Nav1.6<sup>fl/fl</sup> (cyan). (C) Representative image of hind limb strength assay. (D) Latency  
 1184 to fall was quantified. Nav1.6<sup>het</sup> (p=0.999), Nav1.6<sup>cKO</sup> (p=0.797) compared to Nav1.6<sup>fl/fl</sup>. (E)  
 1185 Representative images of grip reflex assay on forelimbs (left) and hindlimbs (right). (F) Mice were  
 1186 assayed on grip reflex. Nav1.6<sup>het</sup> (p=0.999), Nav1.6<sup>cKO</sup> (p=0.351) compared to Nav1.6<sup>fl/fl</sup>. (G)  
 1187 Representative image of hind limb angle quantification. (H) Quantification of mean hindlimb angle.  
 1188 Nav1.6<sup>het</sup> (p=0.389), Nav1.6<sup>cKO</sup> (p=0.021) compared to Nav1.6<sup>fl/fl</sup>. Behavioral testing on mice age  
 1189 P14. N=17 Nav1.6<sup>fl/fl</sup>, N=15 Nav1.6<sup>het</sup>, and N=16 Nav1.6<sup>cKO</sup> (I) Representative images from limb  
 1190 coordination assay. Mice were scored based their ability to grasp the metal grate (top picture shows  
 1191 successful grasp, bottom picture shows foot slip). (J) Quantification of limb coordination score in  
 1192 P14 mice. N=17 Nav1.6<sup>fl/fl</sup>, N= 17 Nav1.6<sup>het</sup>, and N= 16 Nav1.6<sup>cKO</sup>. Nav1.6<sup>het</sup> (p=0.022), Nav1.6<sup>cKO</sup>  
 1193 (p=0.0002) compared to Nav1.6<sup>fl/fl</sup>. A one-way ANOVA with Tukey's Post-hoc comparison was  
 1194 used to determine statistical significance.  
 1195

1196  
1197



1198 **Fig. S3. Recordings from *Pirt*<sup>Cre</sup>;Nav1.1 mice at late postnatal development (A) P14 to P18**  
1199 **monosynaptic responses from Nav<sub>v</sub>1.1<sup>fl/fl</sup> (cyan), Nav<sub>v</sub>1.1<sup>het</sup> (grey), Nav<sub>v</sub>1.1<sup>cKO</sup> (magenta), and**  
1200 **C57Bl/6J (black). Recordings from conditional mouse line exhibited small monosynaptic responses**  
1201 **compared to age matched C57Bl/6J mice that were not reliably quantifiable.**

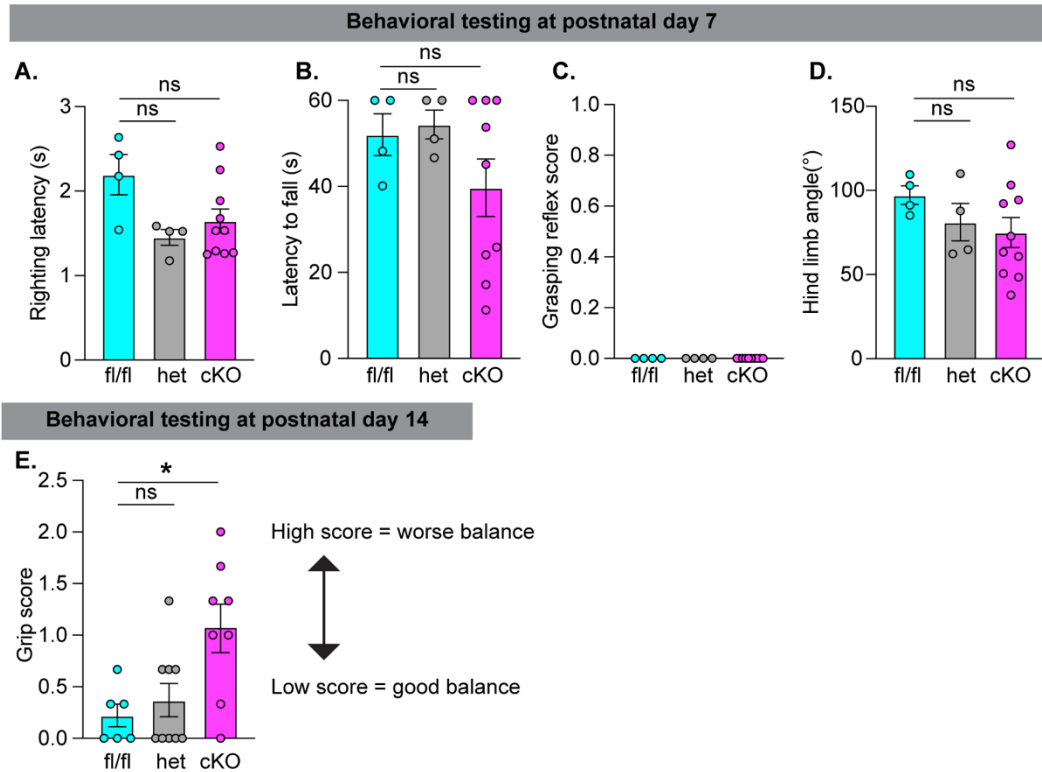
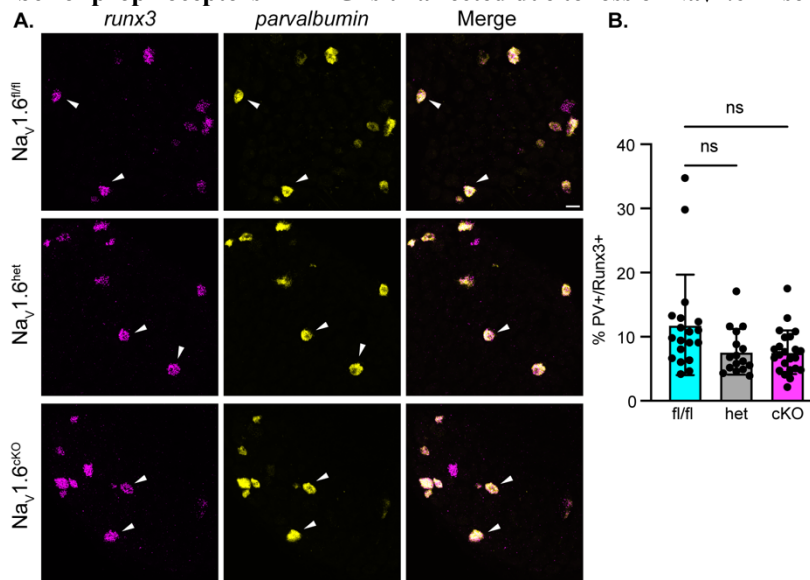


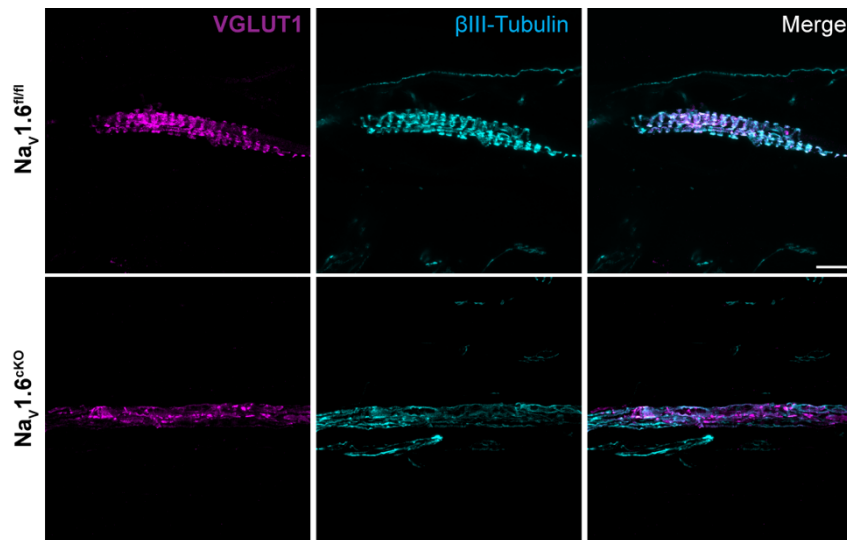
**Fig. S4. Nav1.1 in sensory neurons is required for motor function in late postnatal development.** (A to D) Behavioral testing on mice age P7. N=4 Nav1.1<sup>fl/fl</sup>, N= 4 Nav1.1<sup>het</sup>, and N= 9-10 Nav1.1<sup>cKO</sup>. (A) Latency for mice to right themselves was quantified. Nav1.1<sup>het</sup> (grey, p=0.058), Nav1.1<sup>cKO</sup> (magenta, p=0.142) compared to Nav1.1<sup>fl/fl</sup> (cyan). (B) Latency to fall was quantified. Nav1.1<sup>het</sup> (p>0.999), Nav1.1<sup>cKO</sup> (p=0.715) compared to Nav1.1<sup>fl/fl</sup>. (C) Mice were assayed on grip reflex. All measured values between genotypes. (D) Quantification of mean hindlimb angle. Nav1.1<sup>het</sup> (p=0.637), Nav1.1<sup>cKO</sup> (p=0.906) compared to Nav1.1<sup>fl/fl</sup>. (E) Quantification of limb coordination score in P14 mice. N=6 Nav1.1<sup>fl/fl</sup>, N= 9 Nav1.1<sup>het</sup>, and N= 8 Nav1.1<sup>cKO</sup>. Nav1.1<sup>het</sup> (p=0.845), Nav1.1<sup>cKO</sup> (p=0.015) compared to Nav1.1<sup>fl/fl</sup>. A one-way ANOVA with Tukey's Post-hoc comparison was used to determine statistical significance.

1213

**Fig. S5. The number of proprioceptors in DRG is unaffected due to loss of Nav1.6 in sensory neurons.**



1214 (A) Representative confocal images of Nav1.6<sup>fl/fl</sup> (top), Nav1.6<sup>het</sup> (middle), and Nav1.6<sup>cKO</sup> (bottom)  
1215 adult dorsal root ganglion (DRG) neuron section (25μm). Sections were hybridized with probes  
1216 targeted against parvalbumin (Pvalb, yellow) and Runx3 (magenta). (B) Quantification of the  
1217 percentage of Pvalb+/Runx3+ neurons per genotype. Each dot represents a single DRG section.  
1218 Images were acquired with a 40x, 0.9 NA water immersion objective. A Kruskal-Wallis test with  
1219 Dunn's Post-hoc comparison was used to determine statistical significance. Nav1.6<sup>het</sup> p=0.0694,  
1220 Nav1.6<sup>cKO</sup> p=0.0511 compared to Nav1.6<sup>fl/fl</sup>. N=3 mice for each genotype. Nav1.6<sup>fl/fl</sup> n = 19,  
1221 Nav1.6<sup>het</sup> n=16, Nav1.6<sup>cKO</sup> n =22 sections.  
1222



1223 **Fig. S6. βIII-Tubulin and VGLUT1 labeling in muscle spindles are similar in mice Nav1.6<sup>fl/fl</sup> and Nav1.6<sup>cKO</sup>**  
1224 **mice.**  
1225 Representative confocal images of muscle spindles from Nav1.6<sup>fl/fl</sup> (**top**) and Nav1.6<sup>cKO</sup> (**bottom**)  
1226 adult extensor digitorum longus muscle. Muscle spindle afferents were colabeled with  
1227 VGLUT1 (magenta) and βIII-Tubulin (cyan) antibodies. Images were acquired with 60x, 1.4 NA  
1228 oil immersion objective. Scale bar set to 25 μm.  
1229



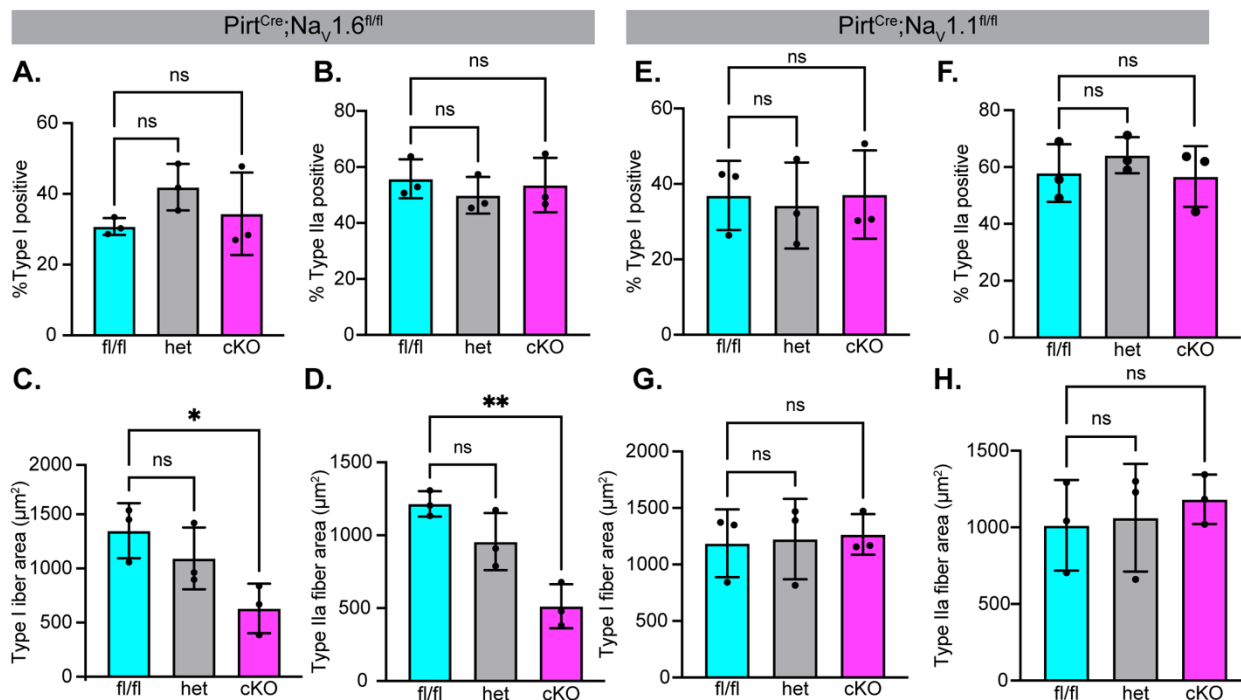
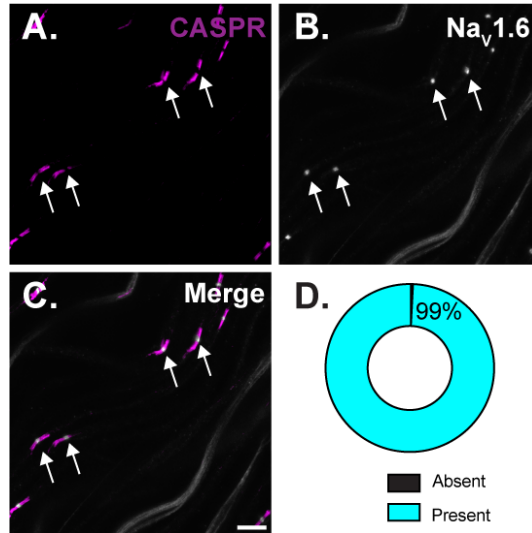


**Fig. S7. Muscle fiber type is unaffected due to loss of Nav1.6 or Nav1.1 in sensory neurons**

(A to D) Quantification of average muscle fiber type in Nav1.6<sup>fl/fl</sup> (cyan), Nav1.6<sup>het</sup> (grey), and Nav1.6<sup>cKO</sup> (magenta). (A) Percentage of type I positive muscle fibers, Nav1.6<sup>het</sup> p=0.2217, Nav1.6<sup>cKO</sup> p=0.8060 compared to Nav1.6<sup>fl/fl</sup>. (B) Type II positive muscle fibers, Nav1.6<sup>het</sup> p=0.5861, Nav1.6<sup>cKO</sup> p=0.9170 compared to Nav1.6<sup>fl/fl</sup>. (C) Type I fiber area, Nav1.6<sup>het</sup> p=0.4209, Nav1.6<sup>cKO</sup> p=0.0250 compared to Nav1.6<sup>fl/fl</sup>. (D) Type II fiber area, Nav1.6<sup>het</sup> p=0.1376, Nav1.6<sup>cKO</sup> p=0.0023 compared to Nav1.6<sup>fl/fl</sup>. (E to H) Quantification of average muscle fiber type in Nav1.1<sup>fl/fl</sup> (cyan), Nav1.1<sup>het</sup> (grey), and Nav1.1<sup>cKO</sup> (magenta). (E) Percentage of type I positive muscle fibers, Nav1.1<sup>het</sup> p=0.9358, Nav1.1<sup>cKO</sup> p=0.9995 compared to Nav1.1<sup>fl/fl</sup>. (F) Type II positive muscle fibers, Nav1.1<sup>het</sup> p=0.9662, Nav1.1<sup>cKO</sup> p=0.6959 compared to Nav1.1<sup>fl/fl</sup>. (G) Type I fiber area, Nav1.1<sup>het</sup> p=0.9819, Nav1.1<sup>cKO</sup> p=0.9236 compared to Nav1.1<sup>fl/fl</sup>. (H) Type II fiber area, Nav1.1<sup>het</sup> p=0.6435, Nav1.1<sup>cKO</sup> p=0.9799 compared to Nav1.1<sup>fl/fl</sup>. A one-way ANOVA with Dunn's post hoc comparison was used to determine statistical significance. Each dot represents a single animal. N=3 for each genotype.

1246



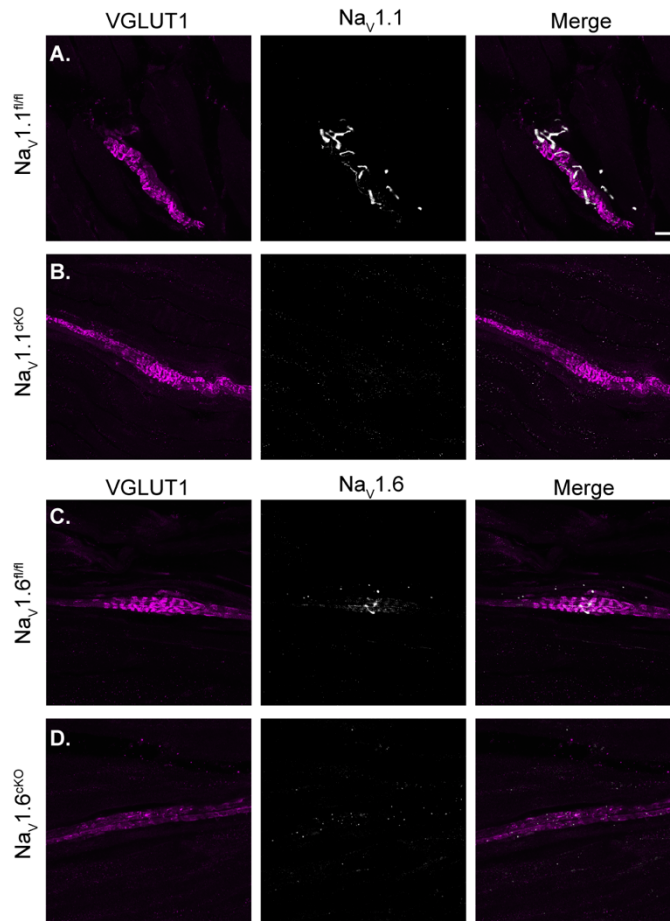
1247

1248

1249

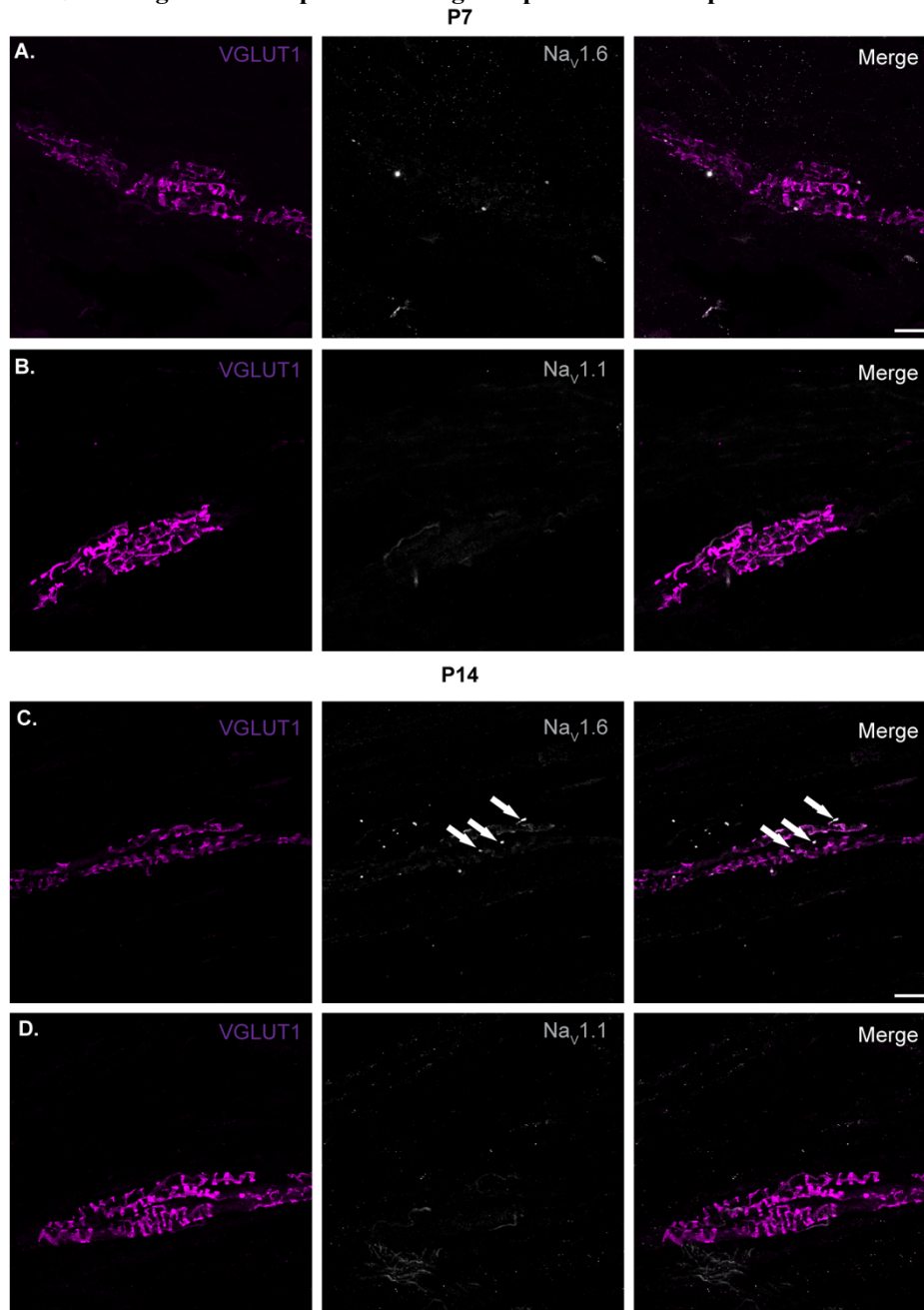
1250

**Fig. S8. Nav1.6 highly expressed at nodes of Ranvier sensory axons.** (A to C) Representative images for sensory nodes of Ranvier were identified via CASPR (A) and Nav1.6 (B) immunoreactivity. (D) Quantification of the percentage of nodes of Ranvier that express Nav1.6. n=247 nodes, N=3 mice. Scalebar=10 $\mu$ m



1251 **Fig. S9. Validation of Nav antibodies targeting Nav1.1 and Nav1.6**  
1252 Representative confocal images of muscle spindles from Nav1.1<sup>fl/fl</sup> (A), Nav1.1<sup>ckO</sup> (B), Nav1.6<sup>fl/fl</sup>  
1253 (C) and Nav1.6<sup>ckO</sup> (D) adult extensor digitorum longus muscle. VGLUT1 (magenta) labels muscle  
1254 spindle sensory endings. Grey scale represents corresponding Nav channel isoform. Scale bar set  
1255 to 20  $\mu$ m. Images were acquired with a 60x, 1.4 NA oil immersion objective.  
1256

1257 **Fig. S10. Nav labeling in muscle spindles throughout postnatal development**



1258 Representative confocal images of Nav1.6 (A, 3= mice, 4= spindles) and Nav1.1 (B, 4= mice, 6= spindles) labeling in  
1259 muscle spindles from extensor digitorum longus muscle from mice at postnatal day 7. Images of Nav1.6 (C, 3= mice,  
1260 7= spindles, arrows denote clusters of Nav1.6) and Nav1.1 (D, 7= mice, 16= spindles) in mice at postnatal day 14.  
1261 Images were acquired with a 60x, 1.4 NA oil immersion objective. All tissue was collected from C57BL/6J mice.  
1262 Scalebar=25  $\mu$ m.  
1263

1264

### Supplementary Table

	P6-P11 vs. P14-P18		
	Nav1.6 <sup>fl/fl</sup>	Nav1.6 <sup>het</sup>	Nav1.6 <sup>cKO</sup>
Latency	0.019**	0.0515	0.8039
Threshold	0.3536	0.2799	0.0027**
Monosynaptic peak amplitude	0.6501	<0.0001****	0.0027**
Polysynaptic peak amplitude	0.1764	0.0002***	0.0032**
FWHM	0.1848	0.8767	0.0002***

1265

1266

1267

1268

1269

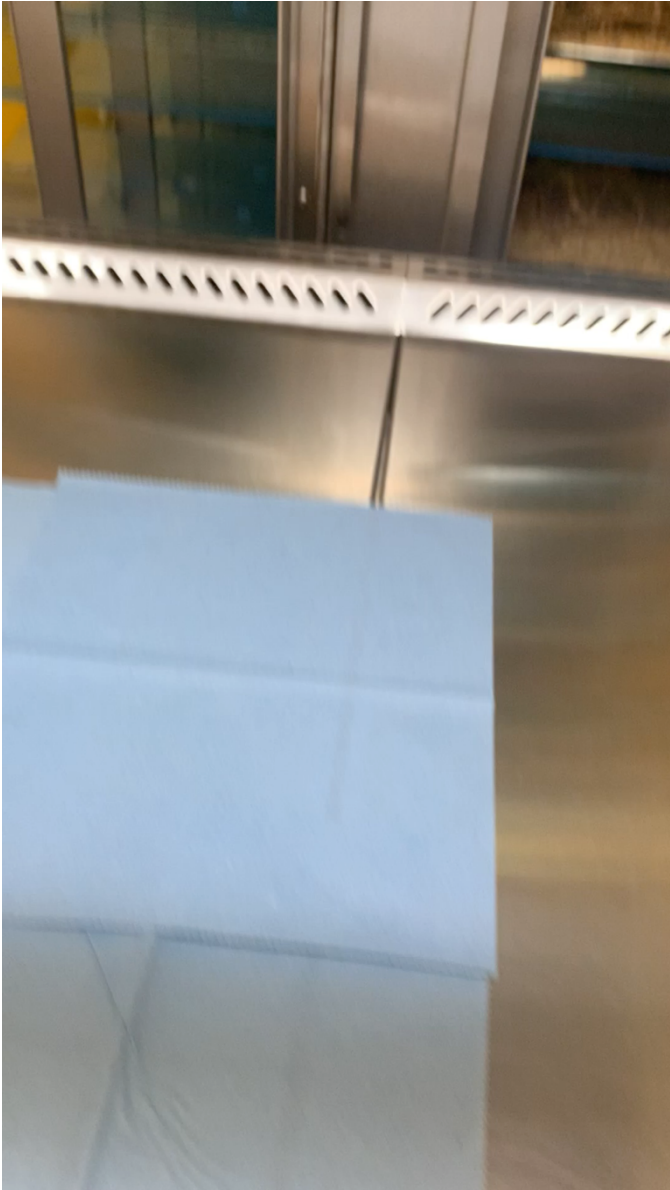
1270

1271

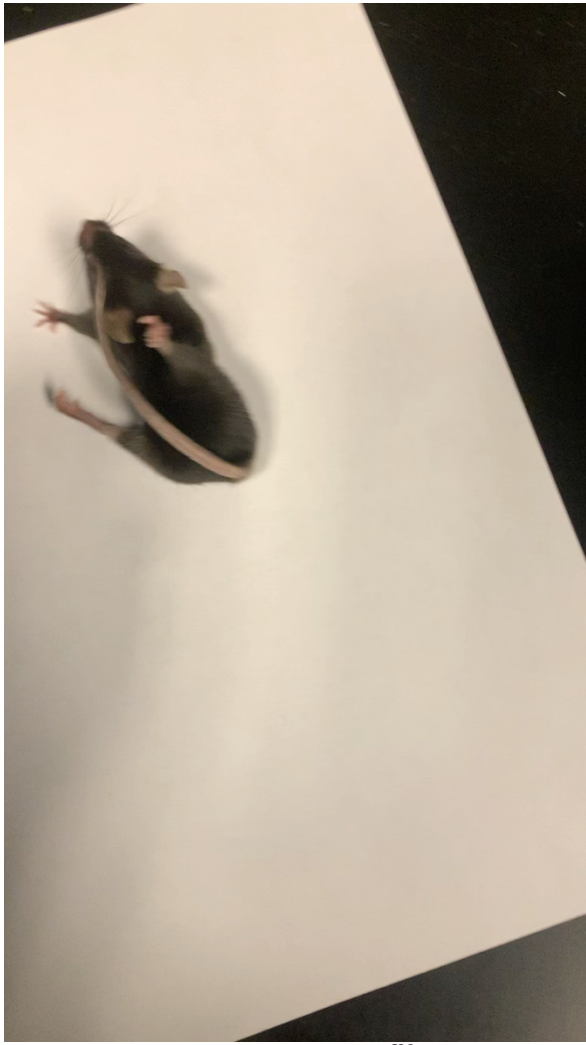
1272

**Table S1: Within-genotype analysis of the monosynaptic reflex response in the Nav1.6 mouse line across postnatal development.** P-values obtained from within genotype, across development, statistical analyses (Two-way ANOVA) of the monosynaptic reflex response in Nav1.6<sup>fl/fl</sup>, Nav1.6<sup>het</sup>, and Nav1.6<sup>cKO</sup> mice.

1273 **Supplementary Movies**



1274 **Movie S1.** Complete loss of limb coordination in Nav1.6<sup>CKO</sup> mice when suspended by tails.  
1275



1276 **Movie S2.** An example of a Nav1.6<sup>CKO</sup> mouse unable hindlimbs or tail to for normal walking behaviors.

1277

1278

1279

1280